

REPORT DOCUMENTATION PAGE			Form Approved OMB NO. 0704-0188		
<p>The public reporting burden for this collection of information is estimated to average 1 hour per response, including the time for reviewing instructions, searching existing data sources, gathering and maintaining the data needed, and completing and reviewing the collection of information. Send comments regarding this burden estimate or any other aspect of this collection of information, including suggestions for reducing this burden, to Washington Headquarters Services, Directorate for Information Operations and Reports, 1215 Jefferson Davis Highway, Suite 1204, Arlington VA, 22202-4302. Respondents should be aware that notwithstanding any other provision of law, no person shall be subject to any penalty for failing to comply with a collection of information if it does not display a currently valid OMB control number.</p> <p>PLEASE DO NOT RETURN YOUR FORM TO THE ABOVE ADDRESS.</p>					
1. REPORT DATE (DD-MM-YYYY) 27-05-2014		2. REPORT TYPE Final Report		3. DATES COVERED (From - To) 21-Jul-2008 - 31-Dec-2013	
4. TITLE AND SUBTITLE Integrated 220 GHz Source Development			5a. CONTRACT NUMBER		
			5b. GRANT NUMBER W911NF-08-C-0051		
			5c. PROGRAM ELEMENT NUMBER 7720T2		
6. AUTHORS Kenneth Kreischer, Jack Tucek, Mark Basten, and David Gallagher			5d. PROJECT NUMBER		
			5e. TASK NUMBER		
			5f. WORK UNIT NUMBER		
7. PERFORMING ORGANIZATION NAMES AND ADDRESSES Northrop Grumman Corporation 7323 Aviation Blvd.  Baltimore, MD 21240 -2001			8. PERFORMING ORGANIZATION REPORT NUMBER		
9. SPONSORING/MONITORING AGENCY NAME(S) AND ADDRESS (ES) U.S. Army Research Office P.O. Box 12211 Research Triangle Park, NC 27709-2211			10. SPONSOR/MONITOR'S ACRONYM(S) ARO		
			11. SPONSOR/MONITOR'S REPORT NUMBER(S) 54511-EL-DRP.13		
12. DISTRIBUTION AVAILABILITY STATEMENT Approved for Public Release; Distribution Unlimited					
13. SUPPLEMENTARY NOTES The views, opinions and/or findings contained in this report are those of the author(s) and should not be construed as an official Department of the Army position, policy or decision, unless so designated by other documentation.					
14. ABSTRACT This report summarizes the technical progress made at NGES during the HiFIVE program developing a 50 W, 220 GHz amplifier based on vacuum electronics technology. Two configurations were investigated: A multi-beam amplifier in a planar magnet and a single-beam device in a cylindrical magnet with radial access. Precision micro-fabrication techniques were used to achieve the stringent specifications for the folded waveguide circuit dimensions and tolerances. We demonstrated high power and good transmission with a five-beam configuration during 2012. Peak output powers up to 21 W were measured at 210 GHz. Even higher powers (55 W) were produced at 214 GHz.					
15. SUBJECT TERMS Submillimeter, vacuum electronics, amplifier, microfabrication					
16. SECURITY CLASSIFICATION OF:			17. LIMITATION OF ABSTRACT UU	15. NUMBER OF PAGES	19a. NAME OF RESPONSIBLE PERSON Kenneth Kreischer
a. REPORT UU	b. ABSTRACT UU	c. THIS PAGE UU			19b. TELEPHONE NUMBER 224-625-4544

## Report Title

Integrated 220 GHz Source Development

### ABSTRACT

This report summarizes the technical progress made at NGES during the HiFIVE program developing a 50 W, 220 GHz amplifier based on vacuum electronics technology. Two configurations were investigated: A multi-beam amplifier in a planar magnet and a single-beam device in a cylindrical magnet with radial access. Precision micro-fabrication techniques were used to achieve the stringent specifications for the folded waveguide circuit dimensions and tolerances. We demonstrated high power and good transmission with a five-beam configuration during 2012. Peak output powers up to 31 W were measured at 219 GHz. Even higher powers (55 W) were produced at 214 GHz because of the higher gain at lower frequencies. A power-bandwidth of 247 W-GHz was measured at 214 GHz, and the overall gain was 28.5 dB. We also achieved a beam transmission efficiency of 75% through the RF circuit to the collector. The multi-beam amplifier is relatively complex, and typically results in a larger and heavier device. We also investigated an alternate concept based a compact single-beam 220 GHz amplifier as part of the HiFIVE program. A prototype was fabricated in 2013, and RF testing resulted in powers up to 19.4 W at 212 GHz with a beam transmission efficiency of 99.5%.

---

**Enter List of papers submitted or published that acknowledge ARO support from the start of the project to the date of this printing. List the papers, including journal references, in the following categories:**

**(a) Papers published in peer-reviewed journals (N/A for none)**

<u>Received</u>	<u>Paper</u>
-----------------	--------------

**TOTAL:**

**Number of Papers published in peer-reviewed journals:**

---

**(b) Papers published in non-peer-reviewed journals (N/A for none)**

<u>Received</u>	<u>Paper</u>
-----------------	--------------

**TOTAL:**

**Number of Papers published in non peer-reviewed journals:**

---

**(c) Presentations**

**Non Peer-Reviewed Conference Proceeding publications (other than abstracts):**

<u>Received</u>	<u>Paper</u>
08/08/2011 6.00	J. Tucek, M. Basten, D. Gallagher, K. Kreischer. A 50 Watt, 220 GHz Power Amplifier, Gomactech 2011. , . : ,
09/03/2013 9.00	Mark A. Basten, John C. Tucek, David A. Gallagher, and Kenneth E. Kreischer. Sub-Millimeter and Terahertz Power Amplifier Development at Northrop Grumman Electronic Systems, Gomactech 2013. 27-MAR-13, . : ,
09/03/2013 10.00	Kenneth E. Kreischer, Jack C. Tucek, Mark A. Basten, and David A. Gallagher. 220 GHz Power Amplifier Testing at Northrop Grumman, IVEC 2013. 22-MAY-13, . : ,
<b>TOTAL:</b>	<b>3</b>

**Number of Non Peer-Reviewed Conference Proceeding publications (other than abstracts):**

---

**Peer-Reviewed Conference Proceeding publications (other than abstracts):**

<u>Received</u>	<u>Paper</u>
08/08/2011 7.00	M.A. Basten, J.C. Tucek, D.A. Gallagher, K.E. Kreischer. 220 GHz Power Amplifier Development at Northrop Grumman, 38th Int. Conf. on Plasma Science. 27-JUN-11, . : ,
08/22/2012 8.00	Jack Tucek, Mark Basten, David Gallagher, Kenneth Kreischer. 220 GHz Power Amplifier Development at Northrop Grumman, Thirteenth IEEE Int. Vacuum Electronics Conference. 24-APR-12, . : ,
09/03/2013 11.00	Mark Basten, Jack Tucek, David Gallagher, Kenneth Kreischer. G-Band Power Module Development at Northrop Grumman, IVEC 2013. 22-MAY-13, . : ,
<b>TOTAL:</b>	<b>3</b>

Number of Peer-Reviewed Conference Proceeding publications (other than abstracts):

(d) Manuscripts

Received      Paper

TOTAL:

Number of Manuscripts:

Books

Received      Paper

TOTAL:

Patents Submitted

Patents Awarded

Awards

Graduate Students

<u>NAME</u>	<u>PERCENT SUPPORTED</u>
FTE Equivalent:	
Total Number:	

Names of Post Doctorates

<u>NAME</u>	<u>PERCENT SUPPORTED</u>
FTE Equivalent:	
Total Number:	

---

### Names of Faculty Supported

<u>NAME</u>	<u>PERCENT SUPPORTED</u>
-------------	--------------------------

**FTE Equivalent:**

**Total Number:**

---

### Names of Under Graduate students supported

<u>NAME</u>	<u>PERCENT SUPPORTED</u>
-------------	--------------------------

**FTE Equivalent:**

**Total Number:**

### Student Metrics

This section only applies to graduating undergraduates supported by this agreement in this reporting period

The number of undergraduates funded by this agreement who graduated during this period: ..... 0.00

The number of undergraduates funded by this agreement who graduated during this period with a degree in science, mathematics, engineering, or technology fields:..... 0.00

The number of undergraduates funded by your agreement who graduated during this period and will continue to pursue a graduate or Ph.D. degree in science, mathematics, engineering, or technology fields:..... 0.00

Number of graduating undergraduates who achieved a 3.5 GPA to 4.0 (4.0 max scale):..... 0.00

Number of graduating undergraduates funded by a DoD funded Center of Excellence grant for Education, Research and Engineering:..... 0.00

The number of undergraduates funded by your agreement who graduated during this period and intend to work for the Department of Defense ..... 0.00

The number of undergraduates funded by your agreement who graduated during this period and will receive scholarships or fellowships for further studies in science, mathematics, engineering or technology fields:..... 0.00

---

### Names of Personnel receiving masters degrees

<u>NAME</u>
-------------

**Total Number:**

---

### Names of personnel receiving PHDs

<u>NAME</u>
-------------

**Total Number:**

---

### Names of other research staff

<u>NAME</u>	<u>PERCENT SUPPORTED</u>
-------------	--------------------------

Mark Basten	0.30
-------------	------

Ken Kreischer	0.40
---------------	------

Jack Tucek	0.40
------------	------

David Gallagher	0.30
-----------------	------

<b>FTE Equivalent:</b>	<b>1.40</b>
------------------------	-------------

<b>Total Number:</b>	<b>4</b>
----------------------	----------

---

**Sub Contractors (DD882)**

1 a. Creatv MicroTech, Inc.

1 b. 11609 Lake Potomac Drive

Potomac MD 20854

**Sub Contractor Numbers (c):** N/A

**Patent Clause Number (d-1):** No patent rights

**Patent Date (d-2):** 9/1/08 12:00AM

**Work Description (e):** Fabricated circuits using LIGA

**Sub Contract Award Date (f-1):** 9/1/08 12:00AM

**Sub Contract Est Completion Date(f-2):** 11/30/13 12:00AM

---

1 a. Creatv MicroTech, Inc.

1 b. 11609 Lake Potomac Drive

Potomac MD 20854

**Sub Contractor Numbers (c):** N/A

**Patent Clause Number (d-1):** No patent rights

**Patent Date (d-2):** 9/1/08 12:00AM

**Work Description (e):** Fabricated circuits using LIGA

**Sub Contract Award Date (f-1):** 9/1/08 12:00AM

**Sub Contract Est Completion Date(f-2):** 11/30/13 12:00AM

---

1 a. Teledyne Scientific & Imaging, LLC

1 b. 1049 Camino Dos Rios

Thousand Oaks CA 913602362

**Sub Contractor Numbers (c):** N/A

**Patent Clause Number (d-1):** No Patent Rights

**Patent Date (d-2):** 9/1/08 12:00AM

**Work Description (e):** Fabricate folded waveguide circuits

**Sub Contract Award Date (f-1):** 9/1/08 12:00AM

**Sub Contract Est Completion Date(f-2):** 11/30/13 12:00AM

---

1 a. Teledyne Scientific & Imaging, LLC

1 b. 1049 Camino Dos Rios

Thousand Oaks CA 913602362

**Sub Contractor Numbers (c):** N/A

**Patent Clause Number (d-1):** No Patent Rights

**Patent Date (d-2):** 9/1/08 12:00AM

**Work Description (e):** Fabricate folded waveguide circuits

**Sub Contract Award Date (f-1):** 9/1/08 12:00AM

**Sub Contract Est Completion Date(f-2):** 11/30/13 12:00AM

---

1 a. Calabazas Creek Research Inc

1 b. 140 W. Franklin St.

Suite 308

Monterey

CA

93940

**Sub Contractor Numbers (c):** N/A

**Patent Clause Number (d-1):** No patent rights

**Patent Date (d-2):** 9/1/08 12:00AM

**Work Description (e):** Fabricated reservoir cathodes

**Sub Contract Award Date (f-1):** 9/1/08 12:00AM

**Sub Contract Est Completion Date(f-2):** 11/30/13 12:00AM

---

1 a. Electron Energy Corp

1 b. 924 Links Ave.

Landisville

PA

17538

**Sub Contractor Numbers (c):** N/A

**Patent Clause Number (d-1):** No patent rights

**Patent Date (d-2):** 9/1/08 12:00AM

**Work Description (e):** Fabricated planar and cylindrical permanent magnets

**Sub Contract Award Date (f-1):** 9/1/08 12:00AM

**Sub Contract Est Completion Date(f-2):** 11/30/13 12:00AM

---

## **Inventions (DD882)**

## **Scientific Progress**

## **Technology Transfer**



# **Integrated 220 GHz Source Development**

## **HiFIVE Final Report**

**July 10, 2008 to December 31, 2013**

**Contract #: W911NF-08-C-0051**

**Prepared for:**

**U.S. Army Research Office (ARO)**

**4300 South Miami Boulevard**

**Durham, NC 27703**

**Submitted by:**

**Northrop Grumman Systems Corporation**

**Electronic Systems Sector**

**Advanced Technology Center (ATC)**

**600 Hicks Road, Rolling Meadows, IL 60008**

The views in this report are those of the authors, and do not reflect the official policy or position of DARPA, the Army Research Office, the Department of Defense, or the U.S. Government. This is in accordance with DoDI 5230.29, January 8, 2009.

---

**Table of Contents**

Executive Summary ..... 1

1.0 Program Objectives..... 1

2.0 Technical Approach and Challenges..... 3

3.0 Phase 1 Technical Results..... 10

4.0 Phase 2 Technical Results..... 26

5.0 Phase 3 Technical Results..... 40

6.0 Findings and Conclusions ..... 48

7.0 Implications for Further Research..... 52

---

## EXECUTIVE SUMMARY

This report summarizes the technical progress made at NGES during the HiFIVE program developing a 50 W, 220 GHz amplifier based on vacuum electronics technology. Two configurations were investigated: A multi-beam amplifier in a planar magnet and a single-beam device in a cylindrical magnet with radial access. Precision micro-fabrication techniques were used to achieve the stringent specifications for the folded waveguide circuit dimensions and tolerances. We demonstrated high power and good transmission with a five-beam configuration during 2012. Peak output powers up to 31 W were measured at 219 GHz. Even higher powers (55 W) were produced at 214 GHz because of the higher gain at lower frequencies. A power-bandwidth of 247 W-GHz was measured at 214 GHz, and the overall gain was 28.5 dB. We also achieved a beam transmission efficiency of 75% through the RF circuit to the collector. The multi-beam amplifier is relatively complex, and typically results in a larger and heavier device. We also investigated an alternate concept based a compact single-beam 220 GHz amplifier as part of the HiFIVE program. A prototype was fabricated in 2013, and RF testing resulted in powers up to 19.4 W at 212 GHz with a beam transmission efficiency of 99.5%. This report will summarize the objectives of the NGES HiFIVE program, the general methodology that was used to address these objectives, the technical problems that were encountered, and the accomplishments that were achieved. A summary of key findings and conclusions will also be provided.

### 1.0 PROGRAM OBJECTIVES

This final report summarizes the technical progress made by Northrop Grumman Electronics Systems (NGES) as a participant in DARPA's High Frequency Integrated Vacuum Electronics (HiFIVE) program. The main goal of HiFIVE was to demonstrate an integrated, microfabricated vacuum electronic (VE) high power amplifier (HPA) at 220 GHz for use in RF transmitters. The key performance objectives were high-power (>50W) and high-bandwidth (>5GHz). This frequency is of interest because it is situated in a broad atmospheric window with relatively low transmission losses. It is generally underutilized and but offers potential system advantages, including wide bandwidth. Realization of a fully-integrated high power amplifier with micro-fabricated circuits at these frequencies could have a significant impact on a variety of defense applications including covert, high data-rate communication, airborne collision avoidance systems, and high resolution SAR imaging during inclement weather conditions.

A significant obstacle to exploiting the spectral region above 100 GHz is the lack of a compact RF amplifier capable of high-power and wide bandwidth. Vacuum electronic HPAs at these frequencies have typically been characterized by poor performance. In addition, the size, weight, and cost of these systems provide challenges for many potential military applications. These features are the result of unfavorable scaling physics that result in the need for very small RF interaction structures that are difficult to fabricate using traditional machining techniques. This has led to HPAs with limited capability. At 220 GHz, for example, the state-of-the-art output power from production HPAs is just a few watts, and the bandwidth is less than 1 GHz. In addition to their limited performance, the complexity and cost of conventionally-machined VE sources has greatly limited their availability. Alternative technologies, such as solid-state MMIC circuits based on InP or GaAs transistors are also in development at these frequencies, but these technologies face their own severe scaling limits and are unlikely to achieve the absolute output power capability of VE devices.

High precision microfabrication technology provides a viable path for making efficient VE interaction circuits with the necessary small dimensions and stringent tolerances required at 220 GHz. For example, Deep Reactive Ion Etching (DRIE) and LIGA processes are potentially capable of manufacturing slow-wave interaction structures at these frequencies with the required resolution and surface roughness characteristics. We investigated both approaches as part of our HiFIVE program. The fabrication of high aspect ratio, metalized silicon circuits using DRIE was done in collaboration with Teledyne Scientific and Imaging (TSI), while LIGA circuits were made by Creatv MicroTech (CMT). Both efforts required significant process development to meet the stringent specifications for waveguide depth uniformity and wall surface finish. Our successful demonstration of high power at 220 GHz confirmed that microfabrication technologies can be exploited in VE devices, and can provide a path for high frequency VE amplifiers with unprecedented performance capabilities.

As part of this program, NGES also investigated a variety of advanced components such as cathodes capable of generating electron beams with a large transverse aspect ratio and high current density, planar permanent magnets, and high power MMIC drivers. This was necessary because of constraints imposed by limitations associated with electron beam compression optics and by the unfavorable scaling of the VE slow-wave structures. For example, the use of high aspect-ratio beams becomes desirable at these frequencies. This includes sheet, annular, and multiple beam configurations. High current density cathodes are also needed because of beam tunnel cross-section limitations. Another significant enabling technology developed during HiFIVE was high power solid-state MMICs that operated at 220 GHz and were used as the first amplification stage our HPA module. The availability of high power reduced the HPA gain requirements, making it easier to achieve stable operation without spurious oscillations.

Thermal management was also an important aspect of our HiFIVE program. The high current density of the electron beam can cause extremely high heat loads, particularly in the RF circuit and in the collector. The primary source of heat in the circuit is due to inadvertent beam intercept on the circuit walls. A considerable effort was spent addressing these thermal issues and attempting to reduce these loads. This included reducing edge emission from the cathode, optimizing the magnetic field to reduce beam deflection, increasing the beam tunnel size as much as possible, and maximizing the collector efficiency. The overall goal was to achieve at least 90% beam transmission from the electron gun to the collector.

Table 1 provides a summary of the Go/N-Go metrics for HiFIVE. Phase 1 had two component goals: demonstration of a high performance beamstick capable of generating a 20 kV high aspect ratio electron beam, and fabrication of an RF circuit that can operate within  $\pm 2\%$  of 220 GHz. The beam had to achieve a current density of  $> 750 \text{ A/cm}^2$ , and 95% had to reach the collector. The goal of Phase 2 was to utilize these components in an HPA, and to demonstrate 50 W over a 5 GHz bandwidth centered at 220 GHz with an overall efficiency of 5%. Phase 3 expanded on the Phase 2 goal by requiring the construction and validation of a fully integrated HPA. This integrated module would include both the driver and the VE amplifier, and thermal management techniques would be incorporated into the module so that high average power could be achieved. More details about these requirements, and the challenges that they posed, will be provided in the next section.

Table 1 – HiFIVE Technical Metrics

Metric	Unit	Phase I		Phase II		Phase III	
		Value	Demo	Value	Demo	Value	Demo
Go/No-Go Metrics							
Beam voltage	kV	20	1A				
Circuit current density <sup>(1)</sup>	A/cm²	750	1A				
Beam aspect-ratio <sup>(2)</sup>		25	1A				
Beam transport efficiency	%	95	1A				
Center frequency accuracy	%	±2	1B				
P <sub>out</sub> <sup>(3)</sup>	W			50	2A	50	3
Bandwidth	GHz			5	2A	5	3
Power-bandwidth product	W*GHz			250	2A	500	3
Efficiency <sup>(4)</sup>	%			5%	2A	5%	3
Total current <sup>(5)</sup>	mA			250 <sup>(6)</sup>	2B	250 <sup>(7)</sup>	3
Additional Metrics							
Spectral purity <sup>(8)</sup>	dBc			-50	2A	-50	3
Driver output power <sup>(3)</sup>	mW			50	2A	50	3

## 2.0 TECHNICAL APPROACH AND CHALLENGES

The basic objective of the HiFIVE program, which consisted of three Phases, was to develop an integrated, microfabricated vacuum electronic HPA circuit for use in high-bandwidth, high-power transmitters, and to demonstrate operation of such a circuit over a 5 GHz frequency band centered at a frequency of 220 GHz. The first Phase focused on the development of a stable, high-power electron beam transport system, and microfabrication of the interaction structure. The second Phase focused on validating a 220 GHz HPA design and developing an advanced, high current density cathode capable of operating without degradation for at least 1000 hours. The third Phase involved the construction and testing of a compact, integrated HPA utilizing the components developed during the earlier Phases. Details about the specific HiFIVE technical goals and challenges, along with our approach for reaching those goals are given below.

### High Aspect-Ratio Electron Beam

A key goal of Phase 1 of HiFIVE was the demonstration of an electron beamstick with an aspect ratio of 25. Previous modeling of a 220 GHz HPA by the Naval Research Laboratory (NRL) indicated that this aspect ratio was needed to achieve an average power of 50 W at this frequency. Possible configurations included a single sheet beam, an annular beam, and a multiple beam array. Stable beam transport was required, with the elimination of parasitic oscillations and beam instabilities, and minimal beam interception in the RF circuit. Because of the complexity of the beam optics, extensive use of modeling and performance simulations was needed to accurately model the beam transport and stability characteristics. The Phase 1 beamstick was designed to be similar to the beam optics configuration of the Phase 2 high power amplifier.

Demonstration of a stable,  $750 \text{ A/cm}^2$  sheet beam with an aspect ratio of 25 was extremely challenging, and required innovative approaches to electron beam formation, magnetics, and beam tunnel structures. The configuration that we selected was a linear array of round electron beamlets. It was felt that this approach provided a means for realizing stable high current-density beam transport through the RF interaction structure. This configuration avoided the instability concerns associated with sheet beams, and was compatible with our multiple FWG circuit concept. While the high current density required for this program still presented challenges, the transport of an array of round beams had the advantage of being relatively well-understood.

Figure 1 shows a schematic of our multiple-beam concept. In the case of an HPA, each of the individual beamlets propagates through a single FWG circuit. For the Phase 1 beamstick demonstration, the circuits were replaced with individual round smooth-wall channels with radii similar to HPA beam tunnels. The individual beam channels extended for 4.8 cm, and had a radius of 110  $\mu\text{m}$ . Each beamlet had a radius in the circuit of 70  $\mu\text{m}$ , and carried 50 mA of current. Beamlets were spaced approximately 2 mm apart. The micro-perveance for each individual beamlet was low, facilitating individual beam focusing and compression, while the overall total beam perveance was consistent with many conventional RF device designs. In this scheme a planar permanent-magnet planar solenoid was used to provide the axial focusing field for the beams. The required magnetic field was 6-8 kG. The biggest challenge with the magnet was minimization of transverse field errors that can cause beam deflection.

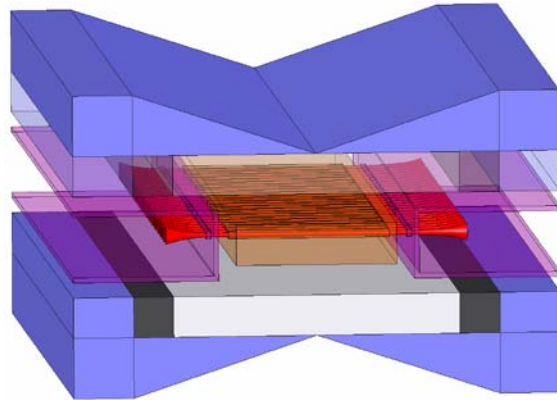


Figure 1 – High aspect ratio beamstick

One of the most appealing aspects of the multiple-electron beam/FWG concept is inherent scalability. In principle the multi-beam concept can be extended to an arbitrary number of beamlets and FWG structures, provided that the magnetics can be fabricated with the required cross-sectional area, and a suitable power combining architecture can be designed. Multiple side-by-side FWG structures can be micro-machined on a common substrate using DRIE micro-fabrication techniques that have been developed. During our HiFIVE program, the biggest challenge for our multi-beam FWG concept was the fabrication of a suitable cathode/gun structure capable of generating multiple electron beams, and the precise registration of that structure to the RF circuit in order to provide for optimal beam transport. We utilized well-developed M-type dispenser cathodes in order to reduce risk. However, the cathode geometry was more complicated, making fabrication and alignment difficult. In addition, our final design required about 20 W of cathode heater power to generate the multiple beams. Single beam TWT cathodes typically operate with 3-5 W of heater power, which results in a simple, more durable heater package. Increasing the heater requirements to 20 W, while keeping the heater package compact, was more difficult than expected. We were able to develop a suitable cathode design during our HiFIVE program, and demonstrated multiple beam generation during Phase 2 of the program, but durability became an issue. More details about cathode performance will be provided in later sections of this final technical report.

The planar, permanent magnet was another challenging component. The magnetics had to be designed to provide confinement and compression of each electron beamlet without deflecting the beam or distorting its cross section. In addition, electrostatic interaction of the beams had to be avoided. In order to achieve these design goals, the ends of the magnet solenoid utilized flux shielding, or cladding, in order to provide a flux-free region at the emitters. Each beamlet had an aperture in the magnet cladding to limit cathode flux and to localize the entrance radial fields for that particular beam-axis for proper beam capture and transport. Design simulations using MICHELLE were performed in order to determine the optimum compression and entrance conditions for individual beam transport. Figure 2 shows a two-beam gun configuration based on this approach. The separation of cathode and beamlets for this case is consistent with the 25-beam beamstick geometry. Since the individual beamlets enter and transit individual beam tunnels, the only beam-to-beam interaction occurs for the short area between the focus electrode and anode/beam tunnel regions. MICHELLE simulations confirmed minimal interaction between the beamlets in our design. Similar simulations were performed for the collector region in order to optimize beam exit magnetics and the depressed collector design. Since the expected circuit efficiency of the FWG device is relatively low (<5%), a single-stage depressed collector was used to improve overall device efficiency. The low circuit efficiency results in a weakly-perturbed beam at the exit of the RF interaction region, which simplifies the collector design and allows for a high collector efficiency (> 90%). The biggest issue for the beam optics after the FWG circuit was the need to expand the high current density beam in order to avoid damaging the graphite collector lens.

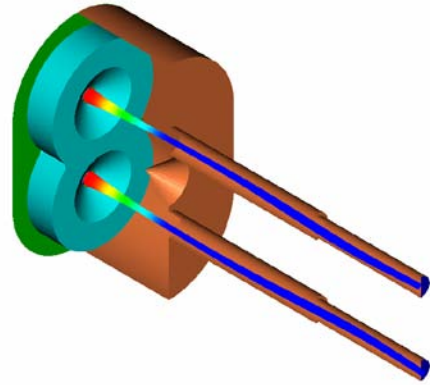


Figure 2- MICHELLE model

### High-Efficiency Interaction Structure

This task involved the design, fabrication, and cold testing of an advanced interaction structure that could efficiently convert energy from the electron beam to the RF field at 220 GHz. The circuit topology needed to be consistent with that of the HiFIVE beamstick. The folded waveguide (FWG) was our choice for the interaction circuit. The FWG circuit, which is shown in Figure 3, has unique characteristics that make it attractive for high power, 220 GHz operation. Its structure is not complex, therefore simplifying the fabrication process. Its planar geometry is compatible with microfabrication techniques. The FWG circuit is also robust, and does not rely on fragile structures such as gratings or posts as part of the slow wave structure to achieve amplification. It can be fabricated from a solid block for excellent thermal management. Finally, tapers at each end of the serpentine waveguide provide an effective way for coupling power into and out of the FWG circuit. NGES has had significant experience with FWG-based amplifiers, and has

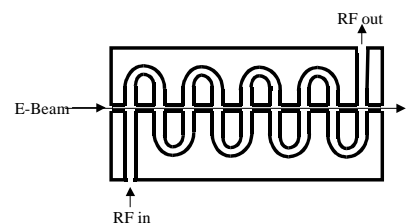
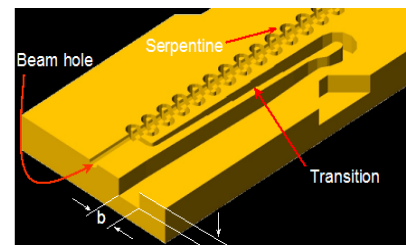


Figure 3 – FWG circuit

implemented this technology in high power amplifiers from 40 to 850 GHz.

A variety of micro-fabrication technologies were considered to make the HiFIVE circuits with precise dimensions and with adequate smoothness of the waveguide wall. We selected metallized silicon circuits using deep reactive ion etching (DRIE) as our preferred approach. This technology is capable of achieving a wall surface smoothness better than 100 nm, which is important to reduce wall ohmic attenuation to acceptable levels. DRIE also is capable of achieving very uniform waveguide depths along the FWG circuit. This is particularly important when power is being combined from multiple amplifier circuits. The RF phase in a given FWG circuit is dependent on the waveguide depth, and minimal phase variation in the circuits is needed for efficient power combining. Our goal was to reduce the waveguide depth variations to  $\pm 2$  microns.

The fabrication of cold test circuits began with extensive 3-D modeling and performance simulations of the electron beam and FWG circuit. Codes that were used included CHRISTINE for the FWG interaction, and MICHELLE for the beam optics. These codes were used to maximize the likelihood of achieving accurate predictions of the beam gain, power and efficiency. After circuits were fabricated, cold tests were performed to validate that the interaction structures were properly made, and that they provided appropriate dispersion characteristics that were consistent with those predicted by the performance simulations. The topology of the interaction structures that were cold-tested closely approximated those required for the HPA. Measurements of transmission/reflection characteristics, as a function of RF frequency, were conducted in order to determine if the circuit had satisfactory attenuation characteristics, as well as minimal mismatch losses. Our measurements indicated that the test circuits met the requirements for wall dimensional tolerances and smoothness needed for a HiFIVE amplifier. Test results are provided later in this report.

### **High Power Amplifier**

The key objective of Phase 2 of HiFIVE was the construction and validation of a 50 W, 220 GHz HPA utilizing the advanced components that were developed during the first phase. In particular, the HPA was to demonstrate an extremely high power-bandwidth product (250 W\*GHz). The HPA demonstration included the validation of all necessary RF circuit elements, including the MMIC first stage driver, FWG circuit, and efficient beam collector. An advanced cathode was not required to achieve the goals of this phase, so we selected well-known M-type dispenser cathode technology for our HPA in order to reduce technical risk. Thermal management was also important because of the need to achieve continuous-wave (cw) operation of the HPA for a minimum of 100 hours.

In order to reduce programmatic risk, we investigated a number of HPA design options. As mentioned earlier, the NRL study that served as the motivation for this program suggested that an aspect ratio of 25 was needed to achieve high average power. This translates into a device with 25 electron beams. We concluded that this would lead to an overly complex VE configuration

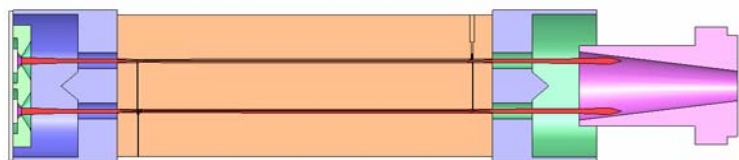


Figure 4— Schematic of a HPA with two FWG circuits

that would be large, heavy, and difficult to build. We also determined that much of the benefit of a multiple beam HPA could be realized with fewer beams. We ultimately selected alternate approaches based on a single beam, as well as a five-beam configuration. The single-beam HPA was based on our successful development of a 650 GHz source during the TIFT program. Initial modeling indicated that a FWG circuit with a single, circular pencil beam could produce powers in excess of 50 watts at 220 GHz. The success of this approach depended on the achievement of high beam transmission through the circuit ( $\geq 90\%$ ). A multiple-beam approach is needed if high beam transmission cannot be achieved. An example of an HPA with two FWG circuits is shown in Figure 4. If beam interception is too high, or localized in the beam tunnel, then circuit damage may occur. A multiple beam approach is attractive because it allows the beam current density to be reduced, lowering the potential for localized damage due to beam interception. But, because of the lack of symmetry, multiple beam systems are more difficult to design and more prone to instabilities. In addition, the RF structures can often support spurious modes, and designing broadband input and output coupling structures is difficult.

Because of the need for cw operation, thermal simulations of the HPA using MAXWELL were conducted to identify the biggest thermal challenges. We concluded that the biggest thermal load was due to beam intercepting the beam tunnel, and not RF ohmic losses. Preliminary calculations of RF ohmic losses indicated a modest 10 degrees rise when the power in the circuit is 50 W. So we focused our attention during the program on minimizing damage due to beam loss. Structures in the beam tunnel were most susceptible to damage. In particular, the high aspect ratio posts formed at the intersection of the folded waveguide and tunnel are fragile and have low thermal conductivity. We attempted to protect these posts by recessing them, as can be seen in Figure 5. The post walls (blue lines) are protected by the non-post walls (red lines), and therefore experience less beam interception. The disadvantage of this approach is that the posts become thinner. Because of the flexibility of DRIE fabrication techniques, it was relatively straightforward to generate these recessed posts.

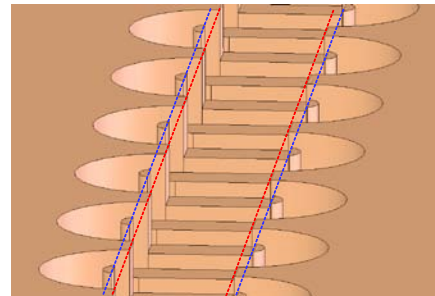


Figure 5 – Recessing the post wall to minimize beam interception

### **High Current Density Cathode**

Another requirement of the HiFIVE program was the development and demonstration of a long-life, extremely high current density cathode. The cathode had to be suitable for integration with the HPA interaction structure. The minimum performance goals of the advanced cathode are listed in Table 1. One essential requirement of the cathode technology was that it be sustainable over a long lifetime (at least 1000 hours). The combination of high current density and long lifetime was very challenging. To achieve  $750 \text{ A/cm}^2$  in the circuit, the density at the emitter needed to be  $30\text{-}50 \text{ A/cm}^2$ . Present dispenser cathodes can achieve these densities but with severely reduced lifetimes. Therefore, two alternate approaches were investigated during our HiFIVE program. The first was a reservoir cathode that was being developed by Calabazas Creek Research (CCR), while the second was a cold cathode based on carbon nanotubes (CNT) being developed by the Jet Propulsion Laboratory (JPL).

CCR has been investigating high current density, controlled porosity, reservoir cathodes using sintered tungsten wires for a number of years. The basic approach consists of small diameter tungsten wires bundled and sintered to form a material with a uniform distribution of parallel pores. The size and distribution of the pores can be controlled by the wire size and sintering time and temperature. This material is sliced perpendicular to the pores to form a thin cap over a reservoir of barium oxide, calcium oxide, and aluminum oxide. In standard powdered tungsten cathodes, the barium compound is impregnated in the porous material, and its diffusion rate is determined by the operating temperature and porosity. To achieve high current density in these cathodes, the temperature is raised to increase barium diffusion to the surface. However, this causes rapid depletion of the barium within the emitter and reduces cathode lifetime. The reservoir cathode addresses the barium diffusion rate by providing control of the porosity by the size, distribution, and length of the pores. The barium compound is stored in a reservoir with significantly larger volume than practical with powdered tungsten cathodes, thereby increasing lifetime. The biggest challenge for the reservoir cathode was fabricating a tungsten wire matrix with consistent pore dimensions. This was particularly important for our multi-beam gun, which needed to generate beamlets with similar current. These fabrication issues were addressed during Phase 1 and CCR did make a prototype cathode, which was tested at the NGS facilities. Results of these tests are provided later in this report.

JPL has been investigating robust, high current density cold cathodes that have low turn-on fields (1-2 V/ $\mu\text{m}$ ). JPL has demonstrated 10 to 15 A/ $\text{cm}^2$  of unfocused current density at fields of 6 to 8 V/ $\mu\text{m}$ . Cathodes are shown in Figure 6. The process of CNT bundle array growth started with catalyst patterning using standard lithography techniques. JPL patterned iron (Fe) in the desired geometry on a conductive silicon substrate. Silicon was the preferred choice because of its conduciveness for micromachining, which allowed shaping of the source, and monolithic electrode integration. The ability to fabricate the desired geometrical arrangement was important for achieving proper beam focusing. After catalyst patterning, the substrate was heated to 650°C in the presence of methane to produce nanoparticles that function as CNT growth centers. The final result is multi-walled CNT bundles with diameters of 20 to 30 nm range. Typically these bundles are grown to a height of about 20 to 30  $\mu\text{m}$ . At such heights, the bundles tend to stay mostly vertical, which is essential for efficient field emission. However, JPL did have problems during our HiFIVE program fabricating vertical emitters on a consistent basis.

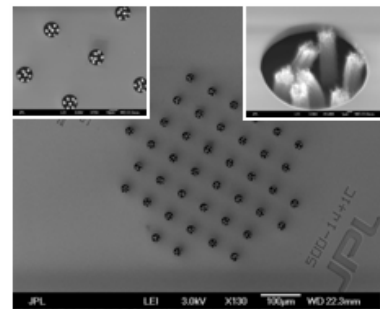


Figure 6 - SEM micrograph of monolithically gate-integrated CNT bundle cathode source.

Transitioning CNT cathode technology from the laboratory to a high average power HPA was also challenging. There are two identified problems with CNT cathodes in terms of lifetime. When the applied field exceeds 10 V/ $\mu\text{m}$  (which is sometimes required to obtain high current densities) the force of attraction exceeded the adhesion strength of CNT bundles to the substrate. As a result, the bundles dislodged from the base and moved towards the anode. Sometimes these bundles became entangled with neighboring bundles, but eventually they separate from the cathode completely. This resulted in a reduction of the emitted current. The second problem, which caused a more gradual decay of the emission

current, was due to sputtering of the anode material that gradually masked emission sites on the cathode. JPL considered incorporating extraction electrodes into the emitter to mitigate this problem. This allowed the placement of the anode far enough from the emitter to prevent the deposition of sputtered anode particles.

### **Fully-Integrated High Power Amplifier**

The original objective of the final phase of HiFIVE was the demonstration of a compact and fully-integrated HPA. This device would incorporate the component technology that was developed during the earlier phases, including an advanced high current density cathode capable of generating a high aspect-ratio beam, a high efficiency interaction structure capable of operating at high current density, and a high power MMIC driver. Metrics for this HPA are given in Table 1. This effort would also include the development cost-effective, efficient methodologies for integrating the various circuit components into a compact HPA. The overall goal was to produce a robust amplifier that would be compatible with military-level production volumes.

Using the technologies developed during the earlier HiFIVE phases, NGES and NGAS had planned to collaborate to fabricate the fully integrated VE amplifier. A key objective was to combine the MMIC driver and interaction structure into a single semiconductor package. This would be beneficial because it would eliminate the die-to-fixture losses in both the MMIC driver and VE amplifier packages, thus reducing the interconnecting waveguide lengths from millimeters to microns. We estimated that this would reduce interconnection losses by ~2 dB, and relieve performance constraints on both the VE circuit gain and the MMIC driver output. This would also significantly reduce the HPA package size by eliminating one waveguide fixture block. We estimated that the HiFIVE source, excluding the magnet, would be approximately 12 cm long, with a cross section of no more than  $2 \times 2 \text{ cm}^2$ .

The integrated HPA concept is summarized in Figure 7. In this scheme, the InP MMIC driver substrate is wafer-bonded directly to a silicon wafer, which has the WR-5 waveguide directly etched into it using DRIE techniques through the Si substrate. An additional trench is etched in the Si substrate for the electron beam tunnel. A second symmetric Si substrate is bonded on top to form the waveguide and interaction structure outline. The waveguide structure is completed by wafer bonding a fourth substrate to the top of the structure to form an enclosed structure containing the MMIC driver and VE interaction structure. This approach to forming the waveguide provides significantly more uniformity than using trenches partially etched into Si substrates. The interior is fully plated to realize a highly uniform, low-loss waveguide with an InP MMIC directly integrated into the die along with the VE interaction structure. A CPW-waveguide transition is integrated at the MMIC input and output. The original Phase 3 plan was to use NGAS's state-of-the-art MMIC fabrication facilities, thus maintaining the performance and quality of the 220 GHz driver MMIC. In addition, a thermal management system was going to be incorporated into the structure to allow the MMIC driver to operate in close proximity to the interaction structure by using dense thermal vias and directly attaching the structure to a plate substrate. If successful, this would have been the first demonstration of a co-fabrication of a transistor-based amplifier and VE interaction structure in a single semiconductor package. We also planned to investigate the possibility of fabricating permanent magnet structures directly into the integrated source. One option, which was proposed by EEC, was to sputter thin film samarium-cobalt on the integrated RF device.

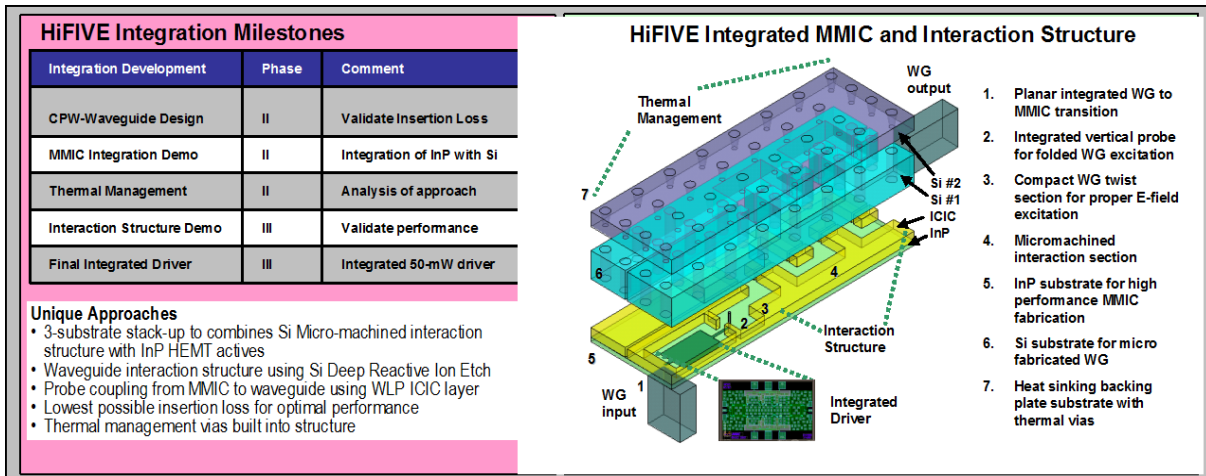


Figure 7 – Summary of Integrated Source Development. The MMIC driver and VE circuit are integrated using advanced micro-fabrication techniques to reduce size and significantly lower interconnection losses

The Phase 3 effort was instead redirected in 2012 to focus on the demonstration of a high average power amplifier rather than an integrated HPA. Operation at 50 W with a multi-beam configuration was demonstrated during Phase 2, but only for short pulses and at low duty. It was felt that operating at high duty (at least 5-10%) would validate the use of micro-fabricated DRIE circuits in VE devices. The program was also redirected to a single electron beam configuration based on our conclusion that a multi-beam approach was not needed to reach the goal of 50 W operation at 50% duty. The single beam HPA that we investigated was based on a radial-access magnet. It is simpler and more compact, but very high beam transmission ( $> 95\%$ ) through the FWG circuit was needed to avoid damage due to beam interception. This required accurate gun alignment and magnets with very low transverse field errors. Operation at 3.2% duty was demonstrated, but power levels were lower than planned because of circuit fabrication difficulties. Test results are summarized in Section 5.

### 3.0 PHASE 1 TECHNICAL RESULTS

The main goal during Phase I of HiFIVE was to demonstrate key sub-components of a compact 50 W amplifier operating at 220 GHz. In particular, we focused on developing a robust folded waveguide (FWG) circuit with low attenuation, and a high aspect ratio beamstick that could generate a  $750 \text{ A/cm}^2$  electron beam that could propagate through the FWG circuit with 95% transmission efficiency. Figure 8 is a conceptual drawing of our 220 GHz amplifier. The device is based on coupled FWG circuits and an electron beam array consisting of multiple separate beamlets. Our design utilizes a micro-machined FWG circuit that was successfully demonstrated during the DARPA TIFT 650 GHz program. The FWG circuit is a robust structure that can be fabricated from a solid block for excellent thermal management. Micromachined input and output couplers serve to split the input drive signal into each FWG circuit and to recombine the amplified signals at the output into a single waveguide. A multiple circuit approach is attractive from a thermal standpoint. Lower beam current is required in each individual FWG in a power combined scheme, resulting in a lower beam tunnel fill factor and reducing the chance for beam interception. However, this approach does require the proper design of an input power splitter

and output combiner to minimize reflections and phase errors. Also, a planar magnet is required with iron pole-pieces that properly focus each of the beamlets.

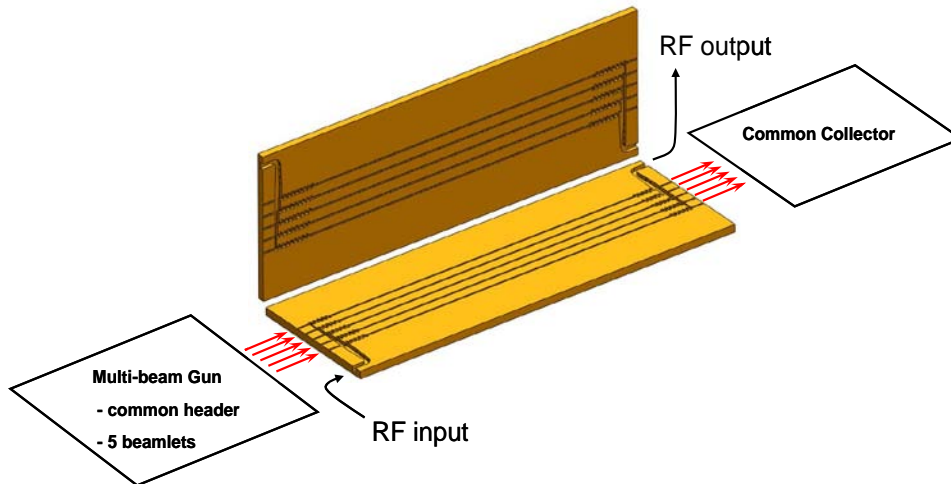


Figure 8 - Five-beamlet 50 W, 220 GHz FWG device.

### **Beamstick Design**

In order to determine the beamstick geometry, slow wave circuit designs were completed capable of achieving >50 W CW at 220 GHz based on CHRISTINE simulations and impedance calculations with HFSS. The expected gain is above 30 dB, so 50 mW of drive power was expected to be sufficient to reach saturation. We began with a trade study, varying the number of circuits required to meet the amplifier metrics. The results are shown in Figure 9. The number of circuits,  $N$ , was varied from 1 to 25. For all values of  $N$ , the output power was kept at about 110 watts, and the beam voltage was about 19 kV. The beam fill factor was made smaller for higher  $N$ . The total beam current increases for higher  $N$ , but the current per circuit decreases significantly. Therefore the gain per unit length decreases and the circuit length must become larger. The total RF input power was assumed to be 50 mW for all the designs. Our study showed that the program goals for output power can be met for a wide range of  $N$ . Fewer circuits have the advantage of shorter length, higher efficiency, and simpler construction (especially for  $N=1$ ). On the other hand, more circuits result in reduced thermal handling requirements because of the lower density of the intercepted current.

Table 2 summarizes a variety of designs that were considered for the 220 GHz amplifier. It also includes the  $N=25$  beamstick parameters. The cut-off frequency and the impedance given in the table were calculated using HFSS. The gain and efficiency were calculated at 220 GHz using Christine 1-D. A variety of beam tunnel cross-sections were analyzed. Dimensions are given in the second and third rows of Table 2. The goal was to make the beam tunnel as large as possible, while maintaining good coupling between the beams and the RF. For low duty, the single circuit device would clearly be the simplest with regard to input/output, magnetics, and construction. However for high duty the maximum temperature in the circuit is over 300°C, which could cause thermal damage. The RF performance of the 25-circuit design is given in Figure 10.

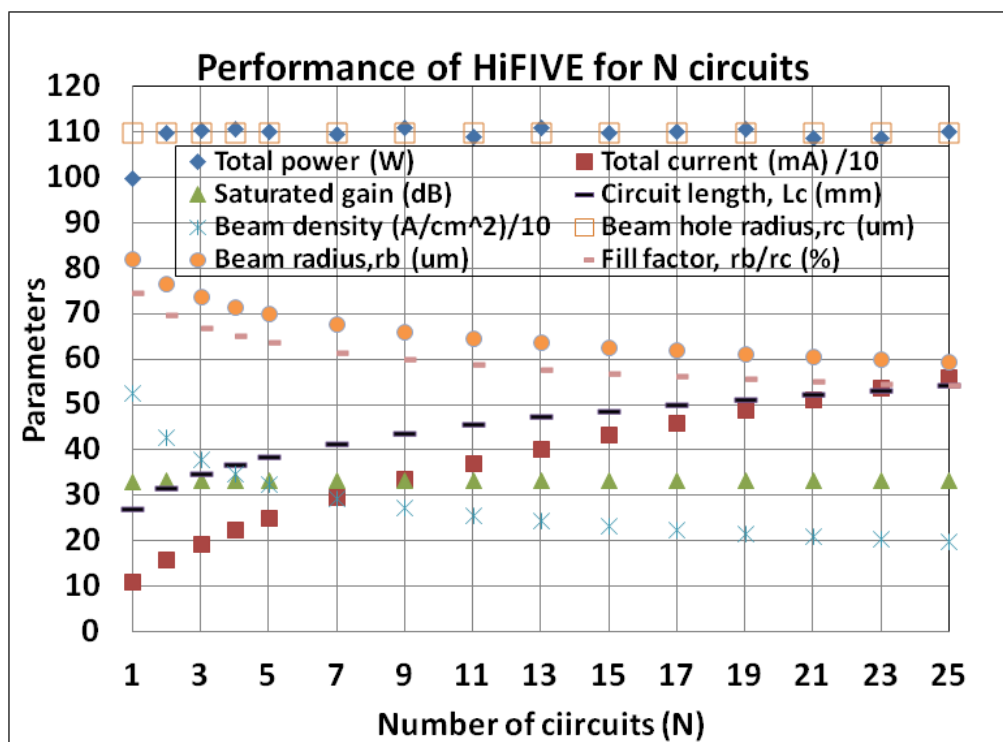


Figure 9 - Characteristics of N-circuit device

Table 2: HiFIVE Circuit Designs

<i>220 GHz Folded WG TWTs</i>	<i>Single circuit</i>	<i>Square</i>	<i>Large rect.</i>	<i>Slot</i>	<i>Large slot</i>	<i>Large square</i>	<i>Beam stick</i>
Circuits (N)	1	5	5	5	5	5	25
Hole along post (μm)	220	168	300	168	200	220	168
Hole into posts (μm)	220	168	168	∞	∞	220	300
Beam radius (μm)	76	50	50	55	70	70	55
Circuit length (cm)	3.43	4.2	4.8	4.8	3.5	4.2	3.52
Beam voltage (kV)	18.25	18.25	18.55	18.25	19.30	19.12	19.00
Circuit current (mA)	130	36.8	50	37	50	50	36.8
Cutoff freq (fc)	198.4	195.7	198.7	206.8	212.8	203.0	212.0
Current density	716	469	357	387	325	325	387
Impedance (ohms)	2.28	3.328	2.484	3.16	2.762	3.037	4.61
Attenuation (dB/cm)	1.88	1.726	1.847	2.91	2.691	2.097	2.655
Total Pout (W)	100	110	171	111	47	150	175
Gain at Pin (dB)	33	33.4	35.3	33.4	29.7	34.8	35.4
Circuit efficiency (%)	4.2	3.28	3.69	5.5	0.97	3.14	1
Bandwidth (GHz)	13	13	8.2	4.6	5.0	8	4.4
Maximum temp(°C)	306	80	108	63	129	202	99

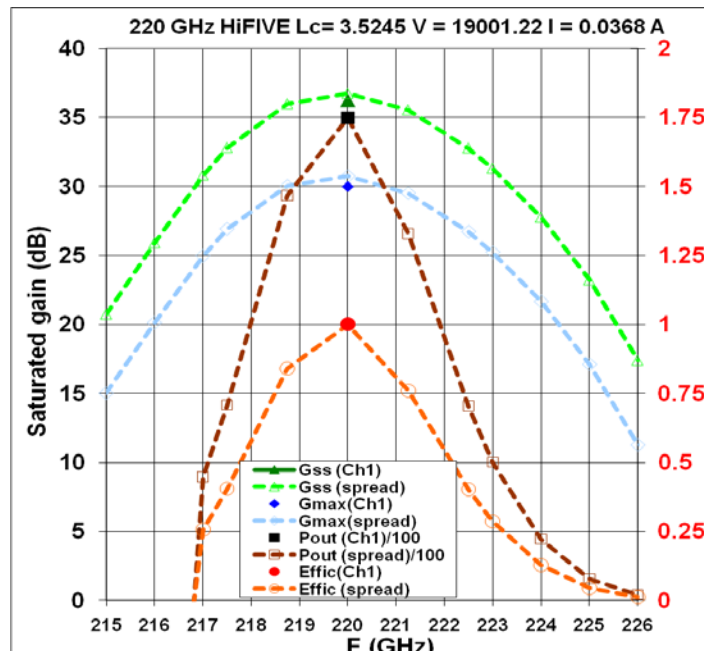


Figure 10 - Performance of the N=25 beamstick design

### Planar Magnet

The HiFIVE beamstick utilized a high aspect-ratio (rectangular-bore) solenoid planar magnet for beam focusing and transport. Figure 11 shows a schematic of the magnet, and a mapping of the axial field in the 0.5 x 4.46 inch bore. The high peak field of 9.6 kG strongly confines the beam and reduces scalloping. MAXWELL simulations of the magnet geometry indicate that a high quality, homogenous field profile can be achieved over the transverse extent of the N=25 linear beam array with an axial flat-field region consistent with the FWG amplifier requirements. Focusing of a linear beam array with area compression of the beam requires a magnetic geometry that is flux-centered around each beamlet axis. This is accomplished with a common pole-piece for flux shielding with round apertures at each beam axis. This has the effect of transforming the magnetic field from the rectangular-bore magnet into an azimuthally-symmetric field profile local to each beam aperture. Such a configuration centers the flux around the individual beam centers and allows for conventional Pierce-like beam optics in the gun region. Additionally, the pole-piece shields the cathode and allows for added flexibility in the cathode axial position relative to the magnet. Additional requirements for the magnet and pole-piece system include an axial field ( $B_x$ ) of approximately 10kG with a flat-field region of at least 2.0 inches, and a homogeneous transverse extent of at least 1.6 inches to account for the beamlet array width. Also, the transverse components of the magnet field ( $B_y$ ,  $B_z$ ) must be extremely low in order to avoid beam intercept along the beam tunnel. Beam optics simulations with the MICHELLE code indicated that the transverse field component in the wide direction ( $B_y$ ) must be less than 30-40 G. Figure 12 shows the basic scheme for a 5-beam case. A high degree of axial magnetic field uniformity was obtained within each pole-piece aperture as well as between apertures, and the local radial magnetic field acquired the requisite symmetry within each aperture.

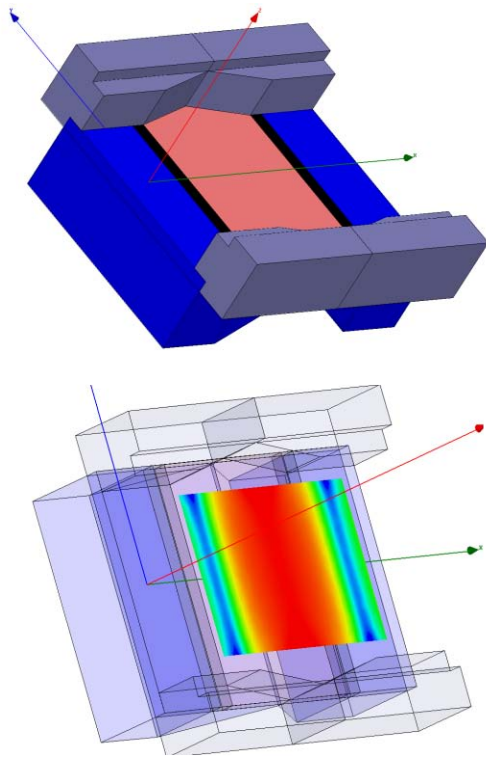


Figure 11 - The baseline high aspect-ratio planar magnet. The top half of the magnet is not shown.

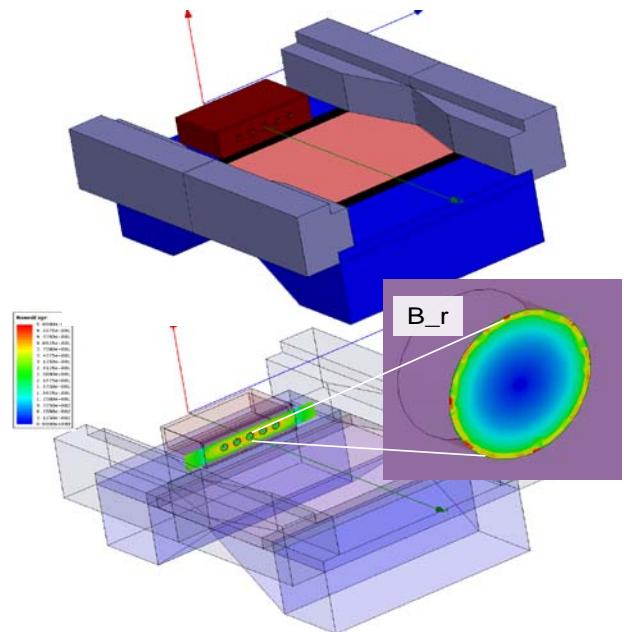


Figure 12 - The high aspect-ratio planar magnet with a five-aperture pole-piece and a linear beamlet array.

Optimization of the planar magnet geometry to reduce transverse magnetic field errors was the focus of a great amount of effort. The most problematic fields are directed in the plane of the wide bore which can deflect the beam and cause interception. The outermost beamlets are most affected since this is where the transverse field errors are largest. Figure 13 shows the expected field errors of the design. The highest fields are in the 20-30 G range. Although small compared to the 9.6 kG axial field the resulting deflection can be problematic because of the small beam tunnel cross section. Further optimization reduced the field near the pole-piece to 10-20 G, which was acceptable based on MICHELLE beam transmission simulations.

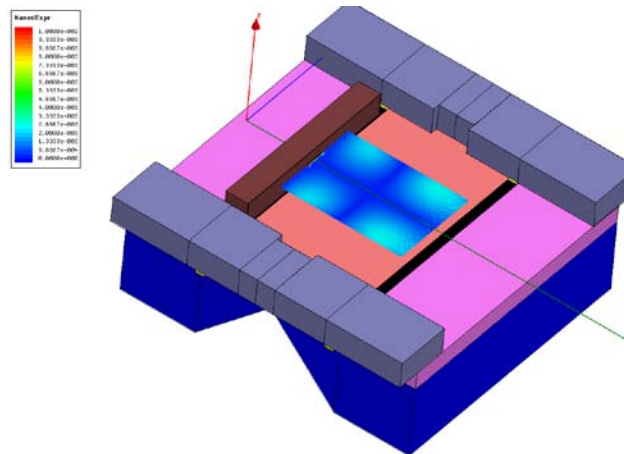
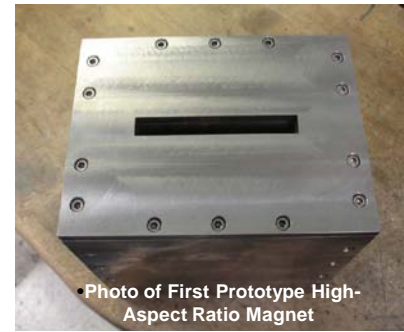


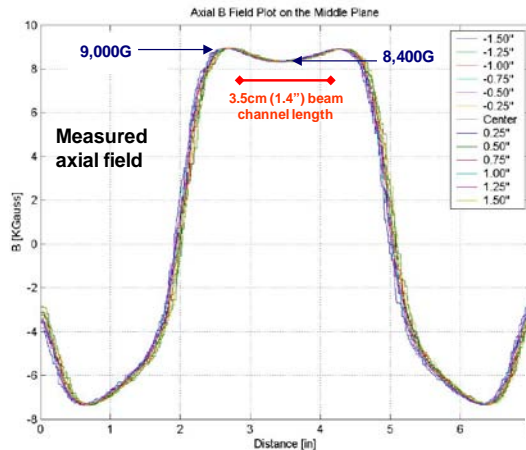
Figure 13 – Transverse field errors

The first prototype of the planar magnet was built by Electron Energy Corporation and is shown in Figure 14. The rectangular-bore magnet has a 9.2kG peak field, bore dimensions of 0.5x5x7" (HxWxL) and transverse error fields on the order of 40-50 G. The second magnet incorporated a number of changes, including the use of higher-saturation permendur in place of iron, which served to reduce the transverse error fields to around 20 G in the beam drift tunnel, consistent with low intercept beam transport. Figure 15 shows the results from a series of field measurements on these magnets. The achieved field profile was much closer to the simulated profile, likely due to the fact that higher-saturation permendur material was used in place of magnet iron for the internal pole-pieces. The first magnet had little saturation margin which allowed additional flux to appear in the magnet center and led to a peaked, rather than flat, magnet profile.



•113 Individual Pieces for Magnet Assembly

Figure 14 - Magnet configuration, individual parts, and completed final assembly.



#### Axial Field Results:

- Profile similar to expected from FEA model
- Obtained adequate field magnitude (9 kG)
- Sufficient axial high-field (~10%) length
- Field ~7% lower than modeled

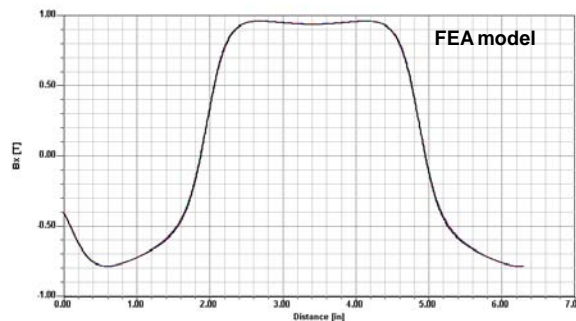
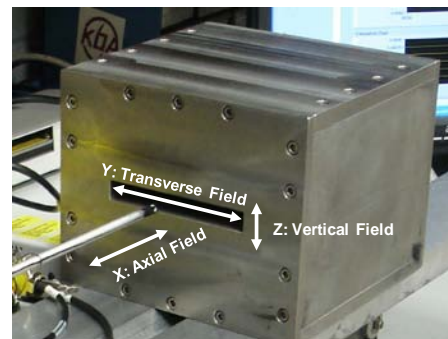


Figure 15 - Second magnet measurements

Great care was similarly exercised in the design of the external shielding pole-pieces. In order to provide margin to magnetic saturation, the outer pole-piece material was switched from Carpenter Consumet iron to a higher field permendur material. Additionally, due to mounting considerations of the beamstick within the pole-piece, we considered the effect of gaps between the anode pole-piece and the surrounding flux-shield. Simulations show that even a 5 mil gap was enough to lead to high magnet field at the cathode ( $\sim 400$  G) and to spoil the beam optics. Due to this concern, we changed the original non-magnetic cupronickel gun can (a part of the vacuum envelope) to a soft magnetic Kovar material. This allowed for the desired field profile in the gun/cathode region to be maintained even in the presence of a 5 mil gap between the pole-pieces. This also resulted in a further reduction of the transverse error field component ( $B_y$ ).

### High Aspect Ratio Beamstick

The goals for the HiFIVE beamstick were to demonstrate an electron beam with an aspect ratio (N) of 25, and to achieve 95% transmission through a FWG circuit with a current density of  $750 \text{ A/cm}^2$ . Our configuration consisted of an array of 25 circular beamlets, each with 0.35 mA of current. A simulation is shown in Figure 16. Because lifetime was not a primary consideration for the beamstick demonstration, the use of a conventional dispenser cathode at elevated temperature was selected as the best approach.

It was less risky than the less developed, and inherently higher risk, advanced cathode technologies required for the Phase II HPA design.

Two hot cathode emitter types were investigated. The first was a standard 411 M-type dispenser cathode fabricated by Semicon. The emitted current density of the dispenser cathode was  $25 \text{ A/cm}^2$ , and required a magnetic area compression of 30. The second type was a barium reservoir cathode configuration based on tungsten wire that was developed by Calabazas Creek Research (CCR). The basic idea of the CCR approach is to braze bundles of tungsten wire together in a side-by-side configuration in order to provide a controlled path for barium to flow from an underlying reservoir to the cathode surface. This “controlled-porosity” approach addresses a long-time challenge in thermionic dispenser cathodes, namely the difficulty in providing an effective diffusion path through the porous tungsten button to the surface. Previous testing at CCR demonstrated over 1000 hrs of cathode life at

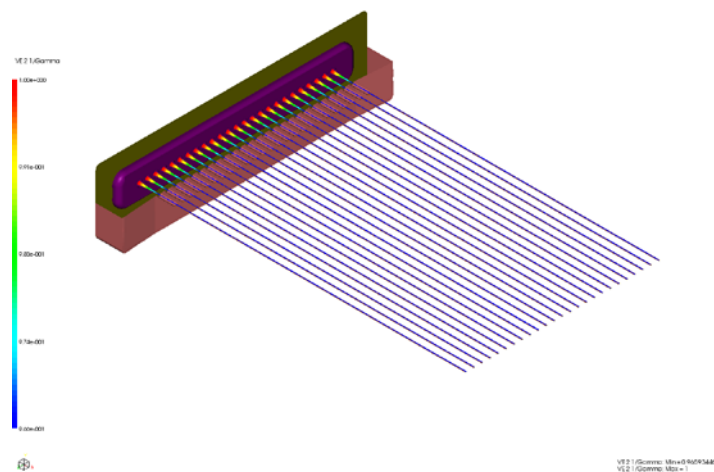


Figure 16 – N=25 cathode simulation

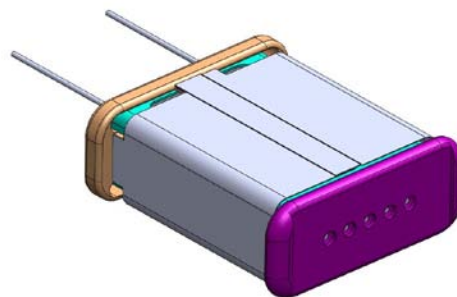


Figure 17 – CCR N=5 cathode

greater than  $50 \text{ A/cm}^2$  emitted current density. Our tungsten wire cathode was designed to operate at  $50 \text{ A/cm}^2$ , and required a magnetic area compression of 15. Predicted beam quality based on MICHELLE simulations was good, with a relatively homogenous beam having  $880 \text{ A/cm}^2$  of beam current density in the beam tunnel. Dispenser emitters were used in a full  $N=25$  array, while CCR built an  $N=5$  array that could be used as a sub-component of the full beamstick. A mechanical drawing of the CCR cathode is shown in Figure 17. Detailed thermal analyses of both guns were conducted to verify that the emitters could be reliably heated to sufficiently high temperature to achieve good emission.

We also investigated cold-cathode carbon nanotubes (CNT) emitters in conjunction with Jet Propulsion Laboratory (JPL). It was felt that cathodes demonstrating over  $25 \text{ A/cm}^2$  could be developed for the HiFIVE Phase II effort. CNT cathodes avoid the thermal problems of hot cathodes, but produce higher emittance beams that could have poorer transmission properties. Early JPL test results indicated sustained emission at  $5 \text{ A/cm}^2$  for low-voltage diode tests. Later cathodes demonstrated  $12 \text{ A/cm}^2$  emitted current during low-voltage testing for over 100 hours of test. A problem that occurred during the HiFIVE program was the detachment of the nanotubes from the substrate in the presence of high electric fields. JPL investigated new techniques to improve the adhesion, and made some progress during Phase 1. However, we decided not to use CNT emitters in the Phase 1 beamstick because of the technical risk. However, because of the JPL progress, a CNT cathode was considered as an option for the Phase 2 high power amplifier.

Validation of our multiple-beam concept was obtained with the 3D beam optics code MICHELLE. The magnetic field structure for the high-aspect ratio magnet was used self-consistently in the simulations to verify proper beam formation and transport could be achieved in the magnet and pole-piece configuration. Figure 18 shows the results of these simulations for the full 25-beamlet array. Full space-charge fields and the effects of thermal electrons ( $T=1125^\circ\text{C}$ ) were included in the simulations. The results show that successful beam transport can be achieved with the flux-centering concept, thus validating the approach.

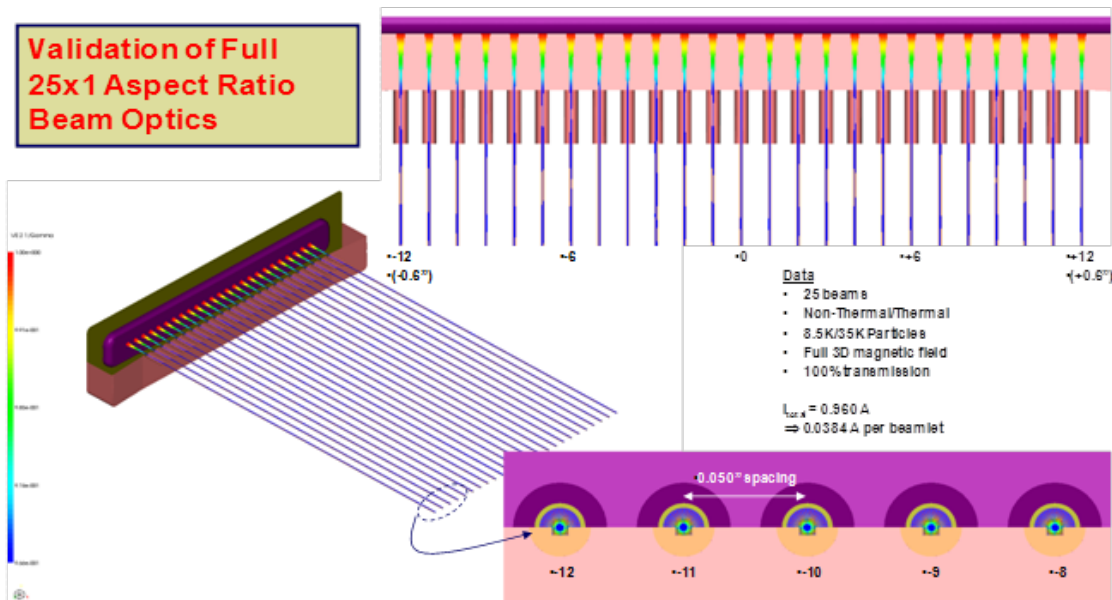


Figure 18 – MICHELLE Simulations

Figure 19 shows the original configuration of the 25-beamlet dispenser cathode. Each beamlet is produced by a separate cathode button, which is either brazed or laser welded into place within an integrated focus electrode assembly. The focus electrode provides electrostatic 'Pierce-like' focusing on each beamlet to produce the desired current density and beam radius for capture in the magnetic field produced by the high aspect ratio permanent magnet. The inner focus electrode insert is made of a tungsten-molybdenum-zirconium (TZM) alloy which helps to inhibit emission from those surfaces. The surrounding outer plate is made from molybdenum. The focus electrode is in electrical and thermal contact with the cathode, and as a result it cannot be separately biased. It also has comparable temperatures to the cathode emitters ( $\sim 1050^\circ\text{C}$ ). Suppression of additional emission from these surfaces was one of the challenges of this configuration. Four cathodes were built by Semicon Associates (SMI) for the Phase I effort.

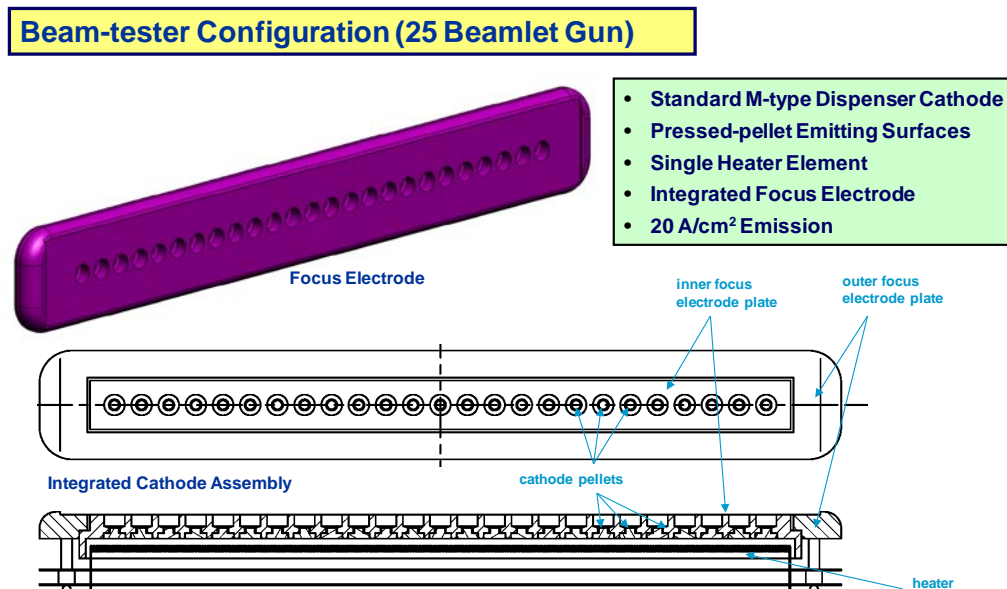


Figure 19 - The 25-beamlet dispenser cathode for the beamstick.

The first cathode configuration was B-type (no M-coating) and utilized cathode buttons which were brazed in place before barium impregnation. Unfortunately little weight gain was observed during the impregnation process, indicating little barium absorption. Subsequent emission testing confirmed poor total emission (only  $10.6\text{ A/cm}^2$ ) at nominal operating temperature. The best emission measured was 370 mA at 13 kV, which is about half of the desired design total. In an attempt to boost the emission the cathode temperature was raised to approximately  $1150^\circ\text{C}$  at higher cathode heater voltage. At this point the heater filament suffered a failure (partial short). This double-wound filament was designed to be non-inductive, resulting in a minimal stray magnetic field at the cathode emitter surface. Later diagnosis revealed the presence of potting voids and a failure point where the highest heater potential occurred between the main and contra-wound filaments. Subsequent analysis indicated that a simpler single-wound filament would be adequate and would only result in a minimal ( $\sim 2\text{G}$ ) stray field at the emitter, so later cathodes used a single-wound configuration. Temperature uniformity was good for the first cathode. The temperature difference across the entire array was an acceptable  $21^\circ\text{C}$ .

The second cathode delivered by SMI incorporated several other changes based on the experience with the first unit. Though still B-type, cathode emitter pellets were now laser welded into place after being impregnated separately in order to boost the barium content. This design required the use of a separate heater, potted into a metal box, which was later mounted to the back of the cathode via a laser weld. Though this resulted in slightly lower heater efficiency, due to the additional interface, the separate impregnation step led to higher emitted current density ( $12 \text{ A/cm}^2$ ) during bell-jar testing. The maximum cathode temperature was limited during bell-jar testing in order to preserve the cathode for subsequent beamstick testing. Results are shown in Figure 20. The highest emission in the bell-jar was obtained at  $1020^\circ\text{C}$ , with  $422\text{mA}$  at  $10\text{kV}$  cathode voltage. One observation was a soft knee characteristic, likely indicative of extraneous emission from the focus electrode as its surfaces became covered with barium because of evaporation from the emitter pellets. Several methods to inhibit surface emission were examined, including the use of zirconium or carbon coatings, but it was decided the risk was too high to implement in view of the short timeframe and limited availability of parts. The path selected for the next beamstick cathode was to utilize M-coating on the pellets to allow for higher emission at reduced operating temperature. This allowed the pellets to emit more preferentially in relation to the focus electrode surfaces. An additional observation about this cathode was a low ( $\sim 20^\circ\text{C}$ ) temperature difference between the center and edge emitter.

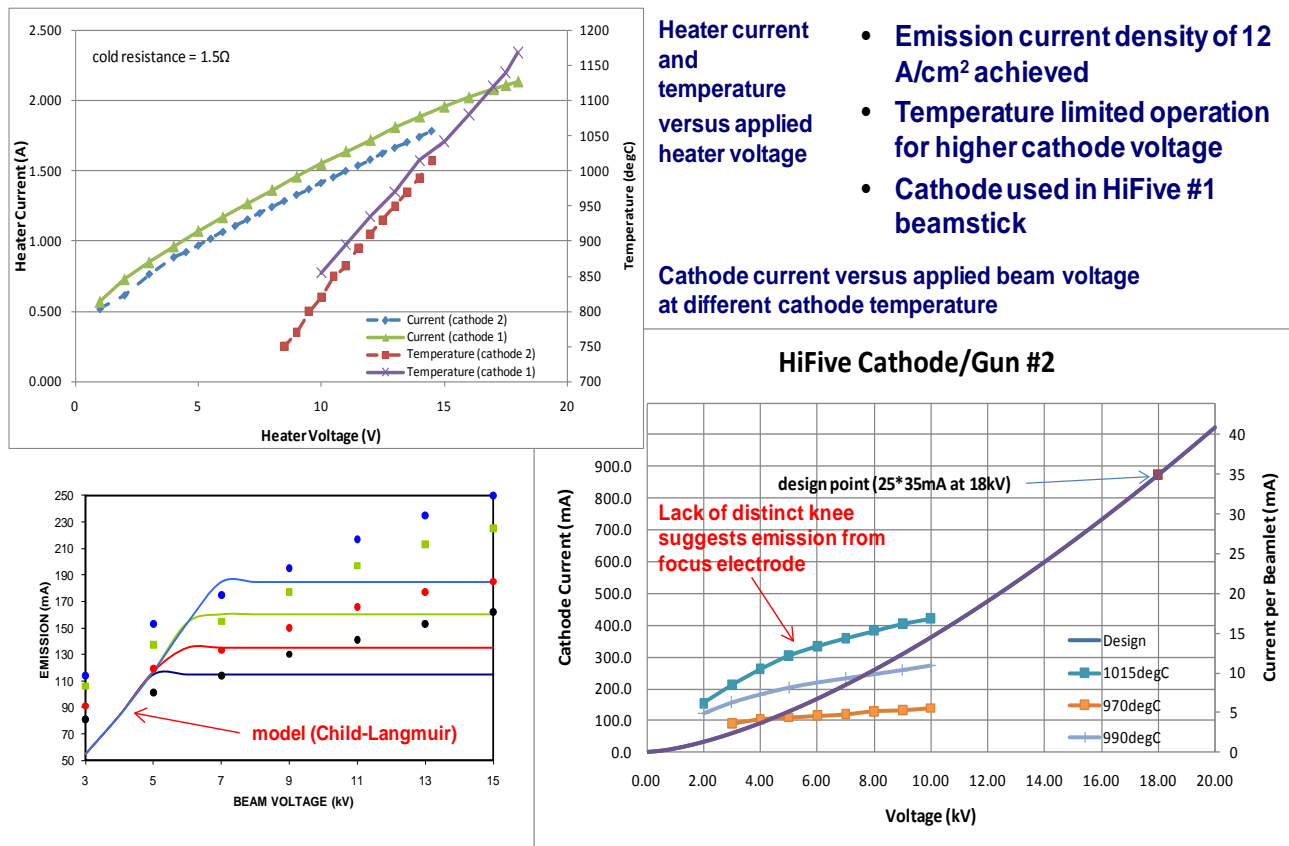


Figure 20 - Measured emission characteristics for cathode #2.

The third cathode configuration was built using M-coated pellets and resulted in a much better space-charge characteristic during emission testing. The cathode temperature was kept at modest levels during the bell-jar testing in order to preserve the cathode for beamstick testing. One unfortunate modification was the welding of the heater box to the back of the cathode at the ends, rather than along the rest of the assembly as in the previous cathode. This was an attempt to boost the cathode heater efficiency, but it had the unintended result of thermally sinking the ends relative to the center, resulting in a high temperature variation (80 °C) across the cathode. This caused the center beams to emit preferentially relative to the outer beamlets. Beam imaging during bell jar tests showed that the inner sixteen beamlets emitted very strongly, while the outer-most edge emitters emitted poorly or not at all. The cathode assembly process was subsequently modified to achieve better temperature uniformity.

We also tested a five-beam cathode based on the CCR controlled-porosity technology. This configuration consisted of a rectangular plate with emitting pellets positioned under a focus electrode. The focus electrode limited emission to the five cathode apertures. We had mixed results during testing because of a fabrication problem during brazing of the focus electrode to the pellet/reservoir assembly. The focus electrode warped relative to the cathode surface during brazing for three of the five emitters. The main impact of this was lower emission from the warped emitter sites. Results from cathode testing confirmed the lower emission, but we were able to verify with copper foil images that two beamlets were formed. We also verified that a low temperature variation was achieved across the five-beam cathode.

While cathode tests were being conducted, a mechanical layout of the beamstick was completed, and can be seen in Figure 21. The same high voltage ceramic was used to support the cathode and collector assemblies. The transmission circuit in the center contained 25 beam tunnels, and had dimensions consistent with the FWG circuit design in Table 2. The collector was electrically isolated in order to measure the transmitted current. A vacuum pump at the end provided the UHV conditions. The beamstick was supported in the bore of the planar magnet on a fixture that was attached to three-axis translation stages that provided both tilt and rotation with micron precision.

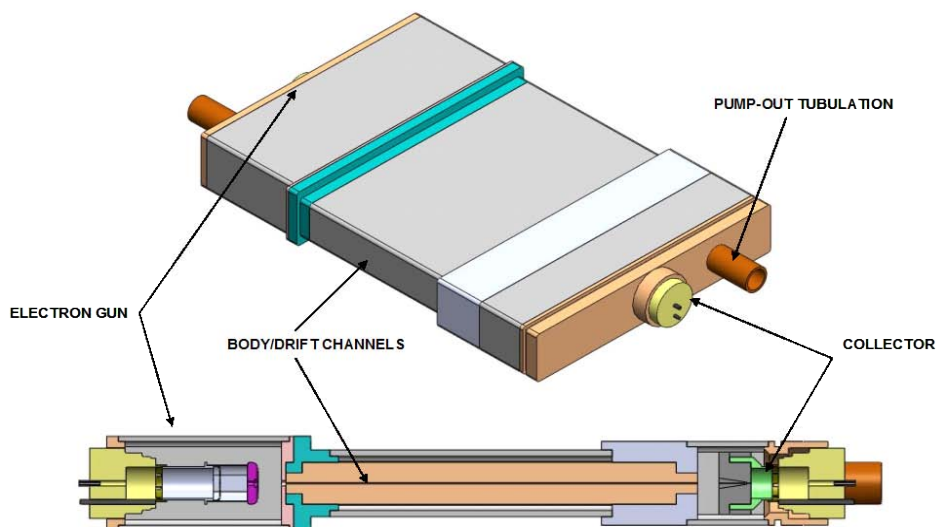


Figure 21 – Beamstick layout

Two beamstick prototypes were fabricated during Phase 1. The first beamstick, built with a dispenser cathode delivered by Semicon, was tested in the planar magnet. The measured cathode emission was found to be low, possibly the result of poor vacuum conditions in the beamstick. We were able to eventually draw about 100 mA of current from the cathode after extended conditioning. We attempted to optimize transmission through the beam tunnel circuit, but were only able to achieve a maximum of 5%. Alignment proved difficult because of the strong magnetic forces on the beamstick resulting from the internal pole-pieces. The next beamstick was fabricated with the M-type Semicon cathode described earlier. Unfortunately this unit developed vacuum leak problems due to assembly problems with the complex mechanical structure, and never made it to final testing in the magnet. The fabrication of a third beamstick began in 2010. It was a five-beam prototype. The change in the number of beamlets was made based on our FWG circuit trade study, and was supported by the DARPA technical team. The goal was to simplify the beamstick and to demonstrate a configuration consistent with the Phase 2 HPA. We attempted to modify the 25-beamlet cathode to meet the HiFIVE requirements, but ultimately decided that a new design optimized for five beamlets was the best path forward. A new cathode was designed and used in HPA testing during Phase 2.

### DRIE Circuit Development

The development of high-efficiency RF interaction structures suitable for a 220 GHz amplifier requires micro-fabrication methods that can achieve the necessary dimensional precision and surface finish. NGC investigated two approaches. The first was based on deep reactive ion etching (DRIE) of a silicon structure followed by metallization. The second was a UV-LIGA technique that used an SU-8 resist and produced an all-copper circuit with better thermal properties. Our analysis indicated that both techniques could meet the dimensional tolerances required for the FWG amplifier circuit. Teledyne Scientific and Imaging (TSI) developed the DRIE processes, while Creatv MicroTech (CMT) focused on the UV-LIGA approach.

DRIE was successfully demonstrated by TSI in the development of a 650 GHz source for TIFT. During TIFT, TSI developed the processes required for fabricating 650 GHz waveguides by aligned bonding of two mirrored wafers, each having metallized trenches formed by DRIE of the silicon substrates. A schematic of the fabrication processes is shown in Figure 22. This technology was developed to meet the following challenging 650 GHz specifications: waveguide aspect ratio ( $\sim 8:1$ ), height/width dimensional accuracy (1%), height uniformity ( $<1\%$ ), sidewall smoothness ( $<50\text{nm}$ ) and top-to-bottom half alignment accuracy ( $<2\text{ }\mu\text{m}$ ). Circuit fabrication constraints, such as those associated with surface roughness and alignment of the circuit halves, were significantly easier to satisfy for HiFIVE at 220 GHz than at 650 GHz. The key differences that required modification of the fabrication processes were the need for a larger waveguide height and a thicker waveguide sidewall metallization. The larger waveguide height required etching deeper Si trenches, to depths of about  $400\text{ }\mu\text{m}$ . DRIE of such deep structures increased the tendency to form unwanted silicon pillars at the bottom of etched trenches. TSI leveraged its expertise in silicon DRIE processes to ad-

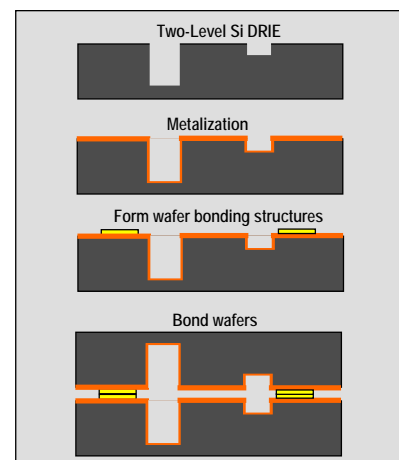


Figure 22 - DRIE fabrication

dress this potential problem. The thicker waveguide sidewall metallization ( $\sim 2.0\ \mu\text{m}$ ) was also a concern. Such metal films can have a thin-film stress that bows the underlying wafer resulting in degraded bonded-wafer alignment accuracy, or creates a gap at the circuit halves. TSI successfully addressed this challenge using its previous experience in the metallization of high aspect ratio structures.

Circuit dimensional errors, in particular variations in the waveguide depth, can cause differences in the phases of the multiple FWG circuits of a HiFIVE HPA. This results in reduced efficiency when combining the RF power at the output of the circuits. Figure 23 shows the dependence of combining efficiency on both phase and waveguide depth (a) variation. The approach that was followed in the development of our multi-beam amplifier circuit was to focus on reducing the overall etch depth variation to less than  $0.7\ \mu\text{m}$ , and hence the phase error to less than  $40$  degrees. This results in a combining efficiency of  $93\%$ . Initial etching experiments with a pure silicon wafer exhibited a  $5\text{--}6\ \mu\text{m}$  variation in the etched depth of the FWG, which was clearly unacceptable based on Figure 23. The etch depth variation was minimized by transitioning from pure silicon to silicon-on-insulator (SOI) wafers. These wafers have a buried silicon dioxide layer beneath a poly-Si device layer with a precise thickness. This buried oxide layer serves as an etch stop. The use of a SOI wafer allowed us to control the FWG depth to within  $0.5$  microns.

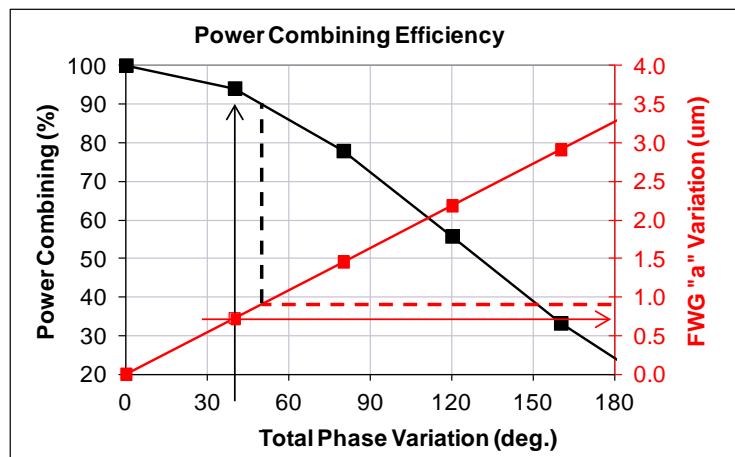


Figure 23 – Power combining efficiency

We began our Phase 1 circuit demonstration by cold-testing a single FWG circuit. This was done to verify that waveguide ohmic losses were acceptable. A comparison of the predicted loss and the actual measurement for the single FWG circuit is shown in Figure 24. The measured loss includes the effects of input and output matches and the loss due to the Chebychev tapers at either end of the FWG circuit. The theoretical calculation is a fit to the data with basically two fitting parameters: the copper conductivity and the roughness of the copper plating. We observed good agreement ( $\pm 0.2\ \text{dB}$ ) between theory and experiment with a copper conductivity of  $5.6 \times 10^7\ \text{1}/\Omega\text{-m}$  and an RMS roughness of  $0.069\ \mu\text{m}$ . The conductivity was consistent with that for high purity OFHC copper, and the roughness was consistent with measurements of TSI's copper plating samples. The actual roughness of the tested FWG could not be measured directly because it was inside the bonded die and therefore not accessible. The FWG attenuation at  $220\ \text{GHz}$  was determined to be  $1.62\ \text{dB/cm}$  based on our cold test data, which met our HPA specifications.

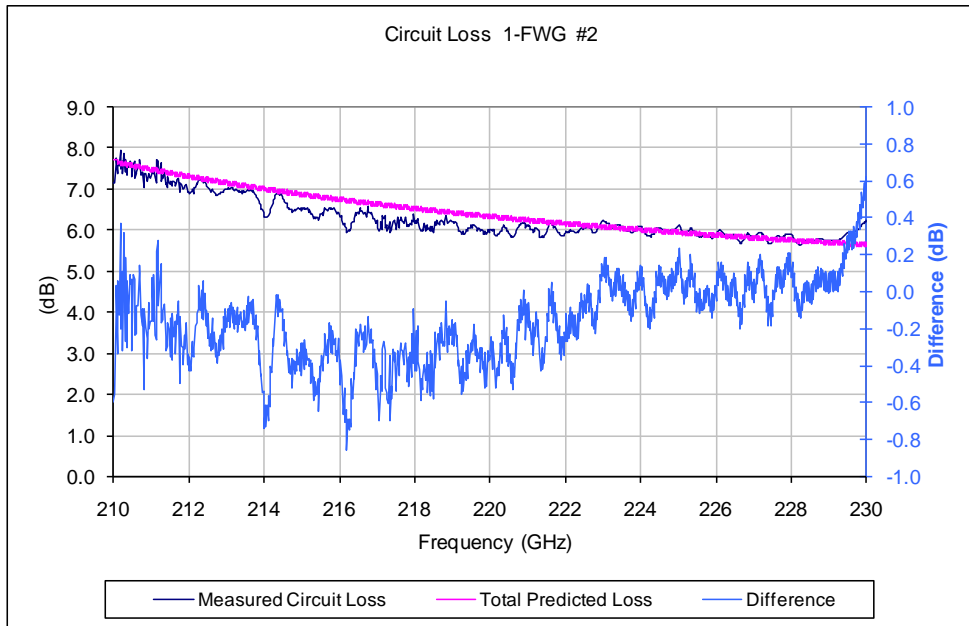


Figure 24 - Total circuit loss for a single FWG circuit.

We also determined the characteristics of multi-FWG circuit configurations. A DRIE cold test circuit consisting of five separate FWGs was fabricated and evaluated. The measured phase difference of each FWG is shown in Figure 25. The total variation in phase from one FWG path to another is about  $40^\circ$  at 220 GHz. A  $40^\circ$  phase error corresponds to a variation in the FWG depth (a) of  $0.73 \mu\text{m}$ , and thus an overall power-combining efficiency greater than 90% based on Figure 23.

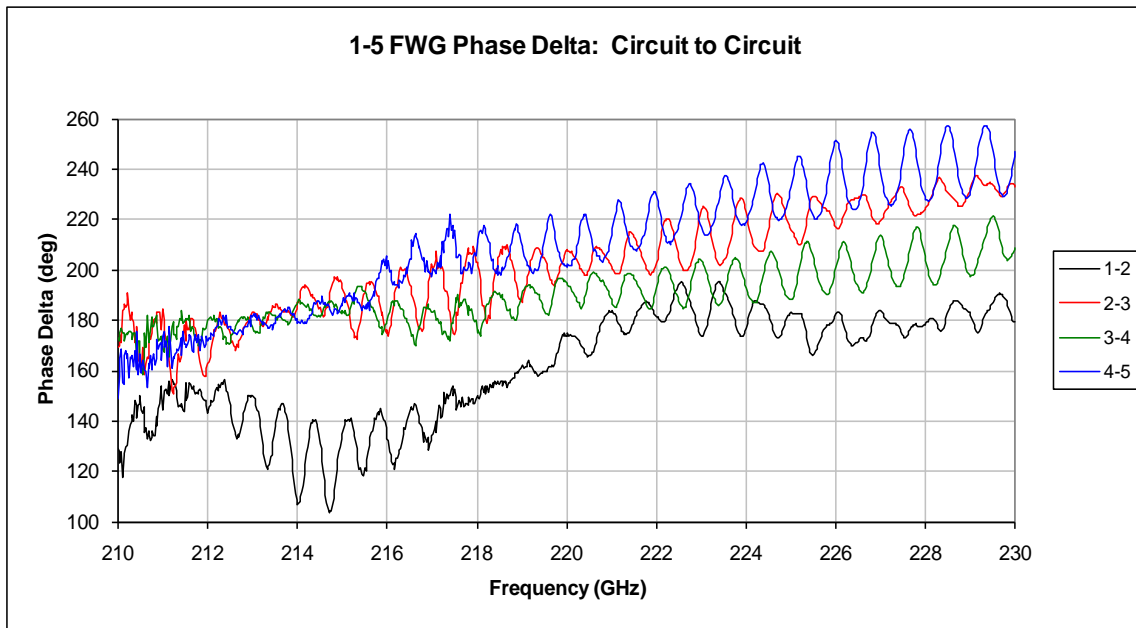


Figure 25 – Measured circuit to circuit phase variation

The total RF loss for a power-combined FWG cold-test circuit was also measured. This circuit had five FWGs. The results are shown in Figure 26. Good agreement was obtained between experiment and theory, with a total measured loss of 7.66 dB at 220 GHz. The theoretical curve is based on an attenuation at this frequency of 1.79 dB/cm. The cold test measurements indicate that there are additional losses, which can be attributed to circuit phase errors. It should be noted that the actual phase errors for this cold test circuit tested are unknown because the individual FWG paths could not be directly measured in the bonded die. We assumed that the phase errors are similar to those measured for the separated FWG circuit (Figure 25), which was produced on the same SOI wafer as the power-combined circuit.

The RF performance of our multi-FWG circuits was verified at NRL in April, 2010. Only small differences (~20% lower copper conductivity) were observed in the measured data. This could be attributed to oxidation of the copper and local testing conditions, like humidity, which may have increased the attenuation. The overall conclusion of the cold tests at NGC and NRL was that HiFIVE multi-FWG circuits fabricated using DRIE could meet the RF specifications required for a 220 GHz HPA.

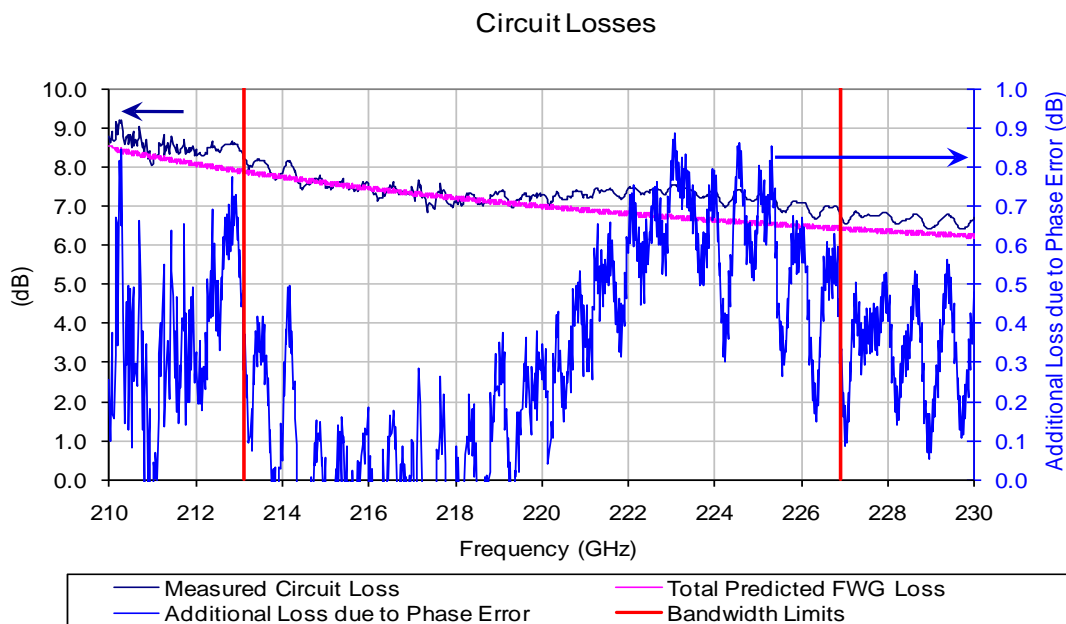


Figure 26 - Power-combined FWG circuit loss

## UV-LIGA Circuit Development

When operating a HPA at high average power, there is concern about thermal damage due to beam interception and high RF power levels. This is especially true for DRIE circuits because of the poor thermal conductivity of silicon at elevated temperatures. Therefore, all-metal circuits were evaluated for use in the HiFIVE amplifier. During Phase 1, Creatv MicroTech (CMT) developed a UV-based LIGA micro-fabrication technique based on a SU-8 photoresist. This tech-

nique was used to produce high aspect ratio FWG circuits that could meet the basic dimensional requirements required for power-combined HiFIVE circuits. SU-8, a negative-tone photoresist, is highly sensitive to UV radiation and has been used in previous high-aspect-ratio micro-fabrication applications. During Phase 1, CMT optimized their UV/SU-8 LIGA process to produce sample circuit halves that were ready to be bonded and RF tested. Figure 27 shows an example of a LIGA circuit half.

The UV/SU-8 LIGA process optimization that occurred during Phase 1 solved many challenges that needed to be overcome to produce useable circuits. Copper coupons, which are used as the base layer for the FWG structures, were planarized with an overall flatness of  $\pm 0.5 \mu\text{m}$ , satisfying the HiFIVE circuit specification. An adhesion of 100% of the post-exposure SU-8 copper structures on the Cu bases was achieved through mask layout, post-exposure bake refinement, and exposure optimization. Defect-free copper plating chemistry was developed without the use of organic leveling compounds in the plating bath. Uniform planarization to achieve parallelism between the bottom of the folded waveguide and the top surface of the circuit die was an area that required considerable attention during Phase 1. Failure to maintain parallelism of the FWG circuit halves results in varying phase along the length of the circuit that reduces the HPA efficiency. While maintaining parallelism, the FWG depth must also be accurate so that the device is optimized at the desired frequency. CMT was able to optimize the necessary fabrication processes to meet the HiFIVE circuit specifications.

Final circuit samples were delivered by CMT to NGC at the end of Phase 1, and they were evaluated. In general they met the HiFIVE circuit specifications. At this point, our focus shifted to the Phase 2 HPA, and the decision was made to base the HPA on the DRIE circuits developed by Teledyne. However, it was felt that the CMT UV-LIGA technology was a promising path forward for achieving high average power. More work will be required to mature UV-LIGA circuit technology. This includes the incorporation of an electron beam tunnel, and the development of techniques for aligning the two FWG circuit halves.

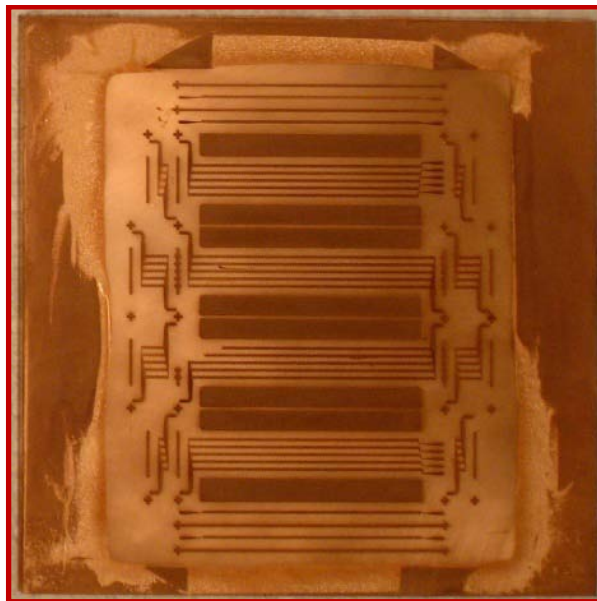


Figure 27 - Planarized LIGA circuits prior to dicing

## 4.0 PHASE 2 TECHNICAL RESULTS

The goal of Phase 2 was to demonstrate a 50 W HPA with a 5 GHz bandwidth centered at 220 GHz and operate with an overall efficiency of 5%. Components that were developed during Phase 1 were to be incorporated into the HPA. In addition, advanced cathodes capable of high current density and long lifetime ( $> 1000$  hours) were to be developed. Our activities during Phase 2 included the completion of a final RF circuit design, generation of a mechanical HPA layout, and fabrication and testing of 220 GHz HPA prototypes.

### Multi-Beam HPA Design

Based on our Phase 1 trade study, which is summarized in Figure 9, we selected a five FWG circuit for our Phase 2 HPA design. This approach resulted in acceptable circuit temperature and reduced the mechanical complexity of the HPA. It was felt that a twenty-five beam configuration that was originally proposed was not needed to achieve high average power, and that the technical risk of that approach was too great. For five FWGs, our thermal analysis indicated that the FWG wall temperature would be about  $100 - 200^{\circ}\text{C}$ , which is acceptable.

Having selected five FWGs for the circuit design, the next consideration was the size and shape of the beam hole. Results of this analysis are shown in Table 2. Beam hole cross sections that were analyzed included a small square, large square, large rectangle, slot, and large slot. The slot is essentially a single beam tunnel shared by all the circuits. A large beam hole is desirable because this increases beam transmission. However, a larger beam hole means lower impedance and consequently the circuit must be longer, which could potentially reduce beam transmission. This reduction in impedance can be offset by designing the circuit so that the cut-off frequency is closer to the operating frequency. This is accomplished by decreasing the FWG depth. However, if the operating frequency is too close to the cut-off frequency, there is too much gain near cut-off, leading to possible spurious oscillations. The slotted circuits in particular have high cut-off frequencies, making them more prone to such oscillations. We selected a final HiFIVE design based on the square beam hole with a  $220 \times 220 \mu\text{m}$  cross section. Circuit parameters are listed in Table 2. The circuit temperature is higher ( $202^{\circ}\text{C}$ ), but circuit damage was not expected. The expected performance of our HiFIVE amplifier is shown in Figure 28. There are two phase taper steps at the end of the FWGs to increase the interaction efficiency

A sever was added near the middle of each FWG. The sever is needed to prevent oscillations due to strong reflections at the RF output combiner. If there is a spurious signal in only one FWG, then the reflection at the power combiner is large and the return loss is high ( $\sim 2$  dB). Our calculations indicated that the net loop gain without the sever was 27 dB, and that the circuit was likely to oscillate. With a sever, stable operation was possible if the attenuation section reduced the signal by at least 11 dB. We considered a number of sever options. Because of the small size of circuit features at 220 GHz, the traditional graphite sever was not feasible. Rather, we utilized the higher attenuation losses of copper waveguide at higher frequency. There was sufficient room for an attenuating section between each active FWG circuit. We designed a sever that provided a total attenuating waveguide path length of 8 cm. The expected attenuation was 2 dB/cm. This resulted in a total loss of 16 dB, which met the stability requirement of 11 dB. We considered increasing the stability margin by modifying the waveguide dimensions of the attenuation section. RF losses can be increased by reducing the waveguide width or by decreasing the FWG

pitch. The disadvantages of these options is the possibility of not fully etching the FWG to the etch-stop, and the formation of very thin structures that are prone to damage. We ultimately decided that the stability margin was sufficient, and kept the waveguide width and pitch constant.

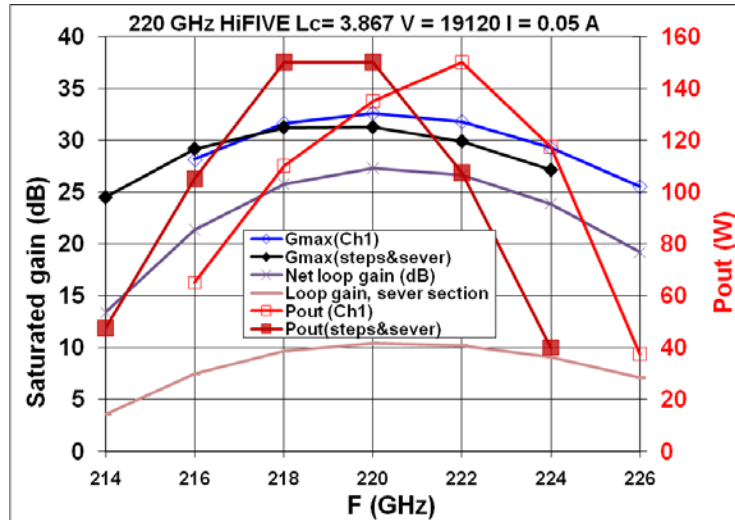


Figure 28 - Simulated performance of the N=5 circuit amplifier

### Input/Output RF Circuit Design

Figure 29 shows the design of the power splitter and combiner for the HPA circuit. This component splits the input signal into five almost equal signals, each of which is the input to one of the five FWG circuits. The same component combines the amplified outputs of the five circuits. The symmetry of the device ensures that the output signals are all combined in the same phase, providing that the electrical lengths of the five FWGs are identical. The I/O circuit consists of a 90° bend, and a three stage impedance transformer to an oversized waveguide, which splits into five waveguides that have the same dimensions as the five serpentine waveguides. The five vertical strips in Figure 29 represent the electron beam tunnels. HFSS simulations indicate that the match is good, with a return loss of about -20 dB over the frequency range of interest. Ideally 20% of the total input power (-7 dB) is transmitted to each of the five arms of the splitter. Results from an HFSS simulation, which are shown in Figure 30, shows this is generally the case, although there is some variation ( $\pm 0.5$  dB) with frequency.

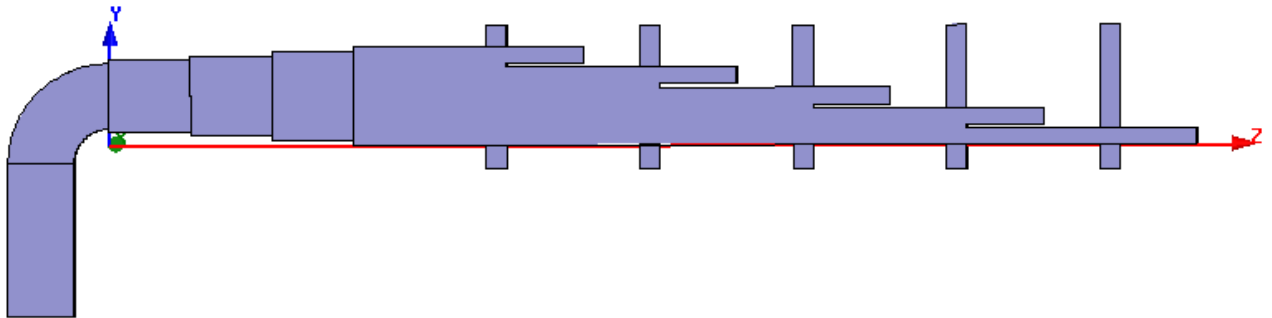


Figure 29 - Design of the power splitter and combiner

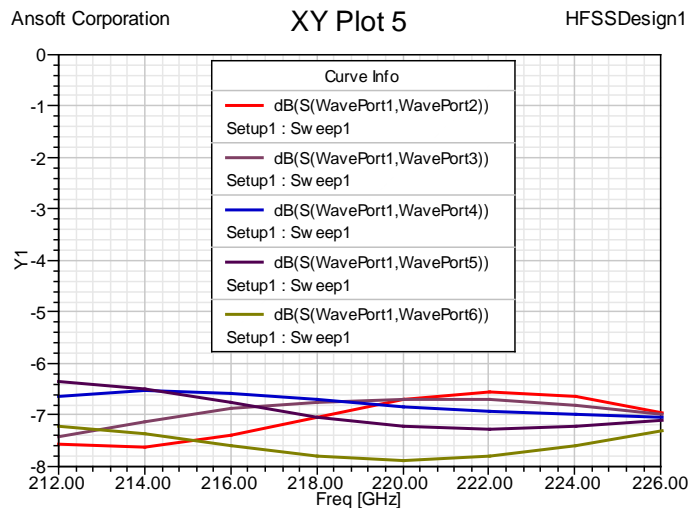


Figure 30: Transmission signal in each of the five circuit inputs

### Circuit Thermal Analysis

A thermal analysis of the HiFIVE circuit was conducted to determine the expected peak wall temperature due to beam interception. Figure 31 shows an ANSYS thermal model of a multi-beam configuration. We assumed 5% electron beam interception loss. Four material layers were used to represent a FWG circuit half. The top layer was the RF circuit, which consisted of silicon metallized with copper. Next was a thin layer of  $\text{SiO}_2$ , which represented the etch stop, followed by another layer of silicon. The bottom layer was copper that contained micro-channels for water cooling. Four channels are shown in Figure 31, and their dimensions are  $1.91 \times 0.51$  mm. The convection coefficient is assumed to be  $2.59 \text{ W/cm}^2/\text{°C}$ , a value calculated from convection cooling equations. The temperature of the water in the cooling channels is  $22 \text{ °C}$ . The highest temperatures occurred at the posts that are formed between the beam tunnel and waveguide. This occurs because these posts are exposed to beam interception, and they have a long thermal path. Figure 31 is an optimistic example with a peak wall temperature of  $80 \text{ °C}$ . However, this temperature strongly depends on the assumptions made about the amount of beam interception and the cooling geometry. More realistic models predicted temperatures of  $100\text{--}200 \text{ °C}$ . We recessed the FWG posts in later circuit designs to avoid thermal damage during high average power operation.

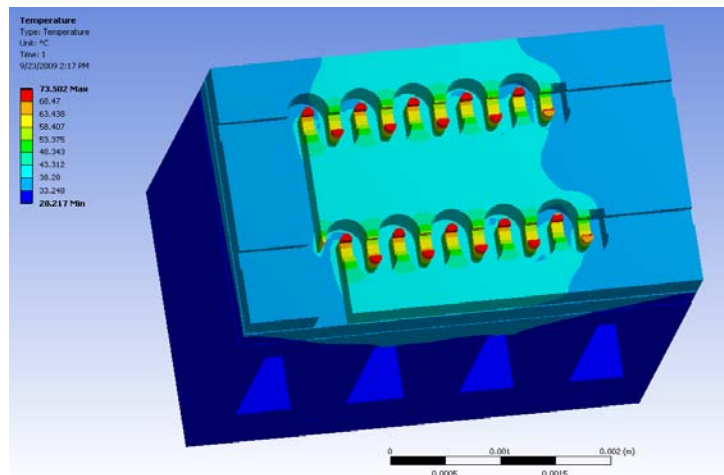


Figure 31 – ANSYS thermal model

## DRIE Circuit Fabrication

Teledyne fabricated the first HiFIVE active circuits using single SOI wafers. These were measured at NGC. It became evident during these measurements that the beam tunnel etching exhibited significant variation in depth both along the circuit from input to center to end and between each individual circuit. The depth variation is shown in Figure 32 for two separate dies. This variation affects the phase along the circuit, and can lead to a reduction in the power combining efficiency. This effect is summarized in Table 3.

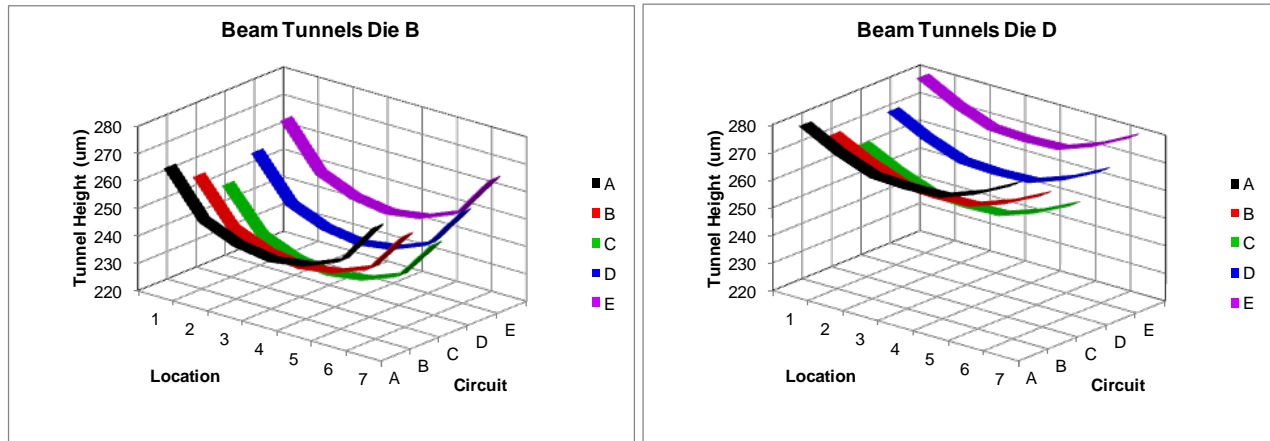


Figure 32 – Beam tunnel variations in two DRIE circuits

Table 3 – Beam Tunnel Variation Measurements

Die	Average Height	Height Variation	Additional Phase Variation	Total Combining Efficiency
B	245.6 $\mu\text{m}$	$\pm 18.5 \mu\text{m}$	$41^\circ - 58^\circ$	75% - 53%
D	267.0 $\mu\text{m}$	$\pm 13.6 \mu\text{m}$	$38^\circ - 56^\circ$	77% - 57%

This result lead to the need to control both the beam tunnel depth and the FWG depth through the use of double-SOI wafers (DSOI). TSI developed additional processing to handle the DSOI substrates and produced effective circuits that were used in testing. While prototypes based on single-SOI and double-SOI wafers were built and tested, the DSOI circuit perform best overall. The use of DSOI wafers has lead to subsequent issues, especially as thermal considerations have become more important. DSOI requires a slightly higher bonding temperature ( $\sim 325^\circ\text{C}$ ) to achieve roughly the same bonding strength as single SOI. However, it was soon learned that the sputtered-gold that was used as a seed layer for the copper plating began to migrate through the copper layer and induce plating roughness and delamination. Based on this finding we began to use a sputtered-copper layer as the plating initiator rather than gold.

## Electron Gun

The HiFIVE amplifier gun used during Phase 2 was based on a Semicon dispenser cathode with a linear array of five emitting elements. A cross-section of the gun is shown in Figure 33. The overall gun design was adequate for demonstrating the amplifier functionality, and achieved good emission and temperature uniformity. However, the cathode heater design for the cathode was not sufficiently robust for long term operation. All five of the cathodes used in the program ultimately failed because of a partial wire short in the heating element. All of the failures were very similar, suggesting a common design problem was responsible. The cathodes were quite large and required significant heat to reach adequate emission temperatures. We typically ran with about 20 W of heater power. It is likely that this high power caused the heating packages to eventually developed internal hot spots that would cause the wire to overheat and break.

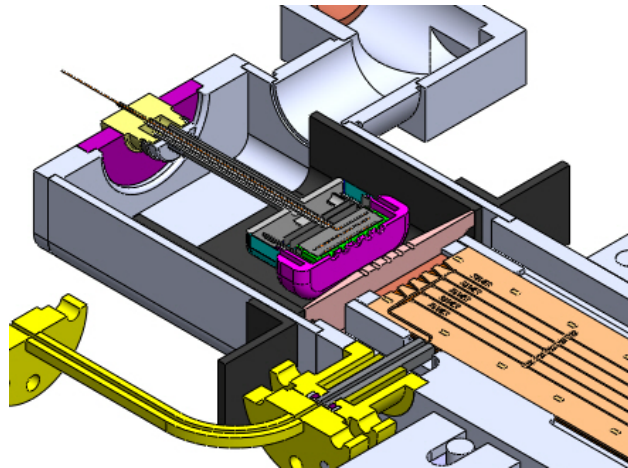


Figure 33 – Cross-section of the multi-beam electron gun

Further development of the heater design was not permitted due to time constraints, but if a multi-beam device is to be pursued in the future, a re-design effort for the cathode heater will be required. Aside from this problem, the M-type cathodes performed well, and exhibited minimal degradation of emission while being operated at emission current densities of  $\sim 20 \text{ A/cm}^2$  for hundreds of hours. The emitting elements were fixtured and laser-welded into place prior to brazing to provide precise, concentric alignment to the integral focus electrode. Thermal isolation within the gun itself was accomplished with molybdenum support structures and thermal shields. The Mo support structures were fragile and required complex EDM to fabricate. The cathode was ultimately mounted on a long (0.9 in) Mo cylindrical rod which was then attached to the brazed gun header assembly. The emitter pellets were fabricated both by conventional machining and EDM. In general, EDM produced a better cathode with better edge definition. Additionally, there were no observed effects of the EDM processing on the emission characteristics.

The focus electrode, shown in Figure 34, was an integral part of the cathode assembly to insure proper alignment of the emitting pellet to the focusing counter-bore for each individual beamlet. Two conditions had to be met with the design of the focus electrode. First, the cross-section of the electrode had to be large enough such that beamlets were unaffected by stray electric fields

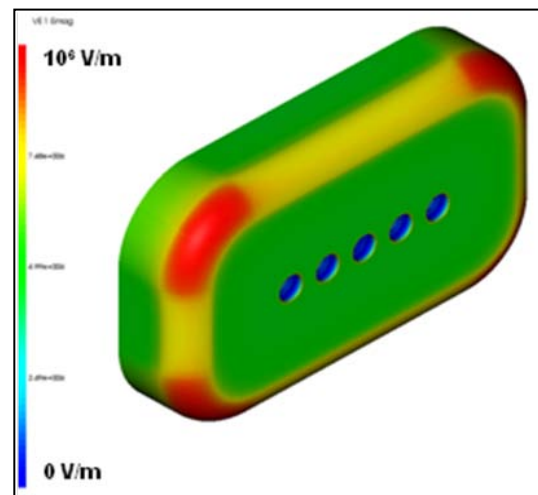


Figure 34 – Gun focus electrode

generated by the electrode edges. Secondly, these edges needed to have large radii of curvature to avoid high voltage breakdown. As a result of these issues, as well as the need to operate at 20 kV, the cathode was relatively large, which led to a large bore for the planar magnet. The highest field gradients occurred at the four corners of the focus electrode as seen in Figure 34.

Assembly of the cathode with the brazed gun header proved to be quite complex and time consuming. Various fixture schemes and alignment techniques were attempted using precision gauge blocks and micrometers. Adequate alignment was typically not achieved upon initial assembly for multiple reasons (part tolerances, material spring-back after welding, etc.), and post-weld mechanical alignment was inevitably required. However, this induced stresses in the cathode mounting parts which later would cause movement when the gun assembly was heated for emission tests. Repeated cycles of alignment and emission testing degraded the emission characteristics, and thus required long cathode conditioning cycles at elevated temperatures, putting additional stress on the heater assembly.

Iron shielding was used to reduce the magnetic flux in the gun region and allow the beamlets to properly focus. This shielding is shown in black in Figure 33. If the  $B_z$  flux (the z-axis is the short axis relative to the gun) is not reduced to less than 25 G at the top and bottom of the cathodes, the beamlet will experience shear that distorts its shape that can cause it to scrape the sides of the beam tunnel, reducing the transmission efficiency. This is seen in Figure 35. In one HiFIVE prototype, a stronger magnetic shield was fabricated from Permendur sheets. While this shielding reduced the beam shear, it also lessened the ability to “steer” the beams because without  $B_z$ , one cannot deflect the beamlets left or right to correct for mechanical misalignments. The inner gun shield was connected to the iron anode which is used to create the radial symmetry about the individual beamlet axes. We concluded that the best method for securing the anode, gun shield, and cupronickel gun can was to shim and laser weld at all possible locations. Differential expansion of the parts during heating at exhaust or when the cathode is operational can cause the welds to break. External iron wings were also used to reduce the error fields ( $\pm B_y$ ) within the beam tunnel region to acceptable levels. More information about the magnetics is provided in the next section.

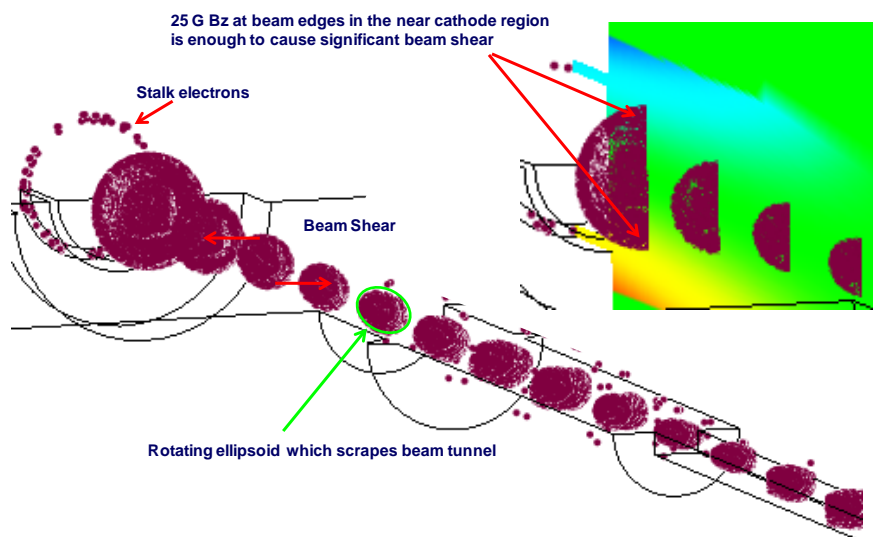


Figure 35 – MICHELLE simulation of a beamlet.

## Magnetics

The 220 GHz HPA required very good beam transport of the five beamlets in order to generate high RF power and to reduce thermal heating of the RF circuit. This in turn required stringent performance of the integrated magnet and shielding system for optimal beam formation, transport and focusing. Specifications for the magnet and pole-piece system included a peak axial field of approximately 6 kG, with a flat-field region that extended axially for two inches and transversely for 0.32 inches. In addition, the transverse magnetic field errors needed to be less than 20 G to avoid beam deflection that could cause excessive beam loss.

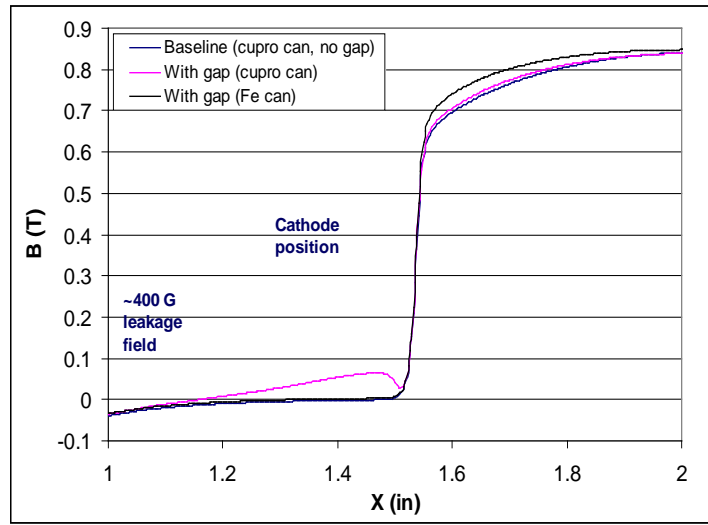


Figure 36 - Simulated cathode axial field with a gap present.

Ideally there should be no magnetic field between the cathode and anode, and then the beamlets should be injected onto five separate magnetic axis formed by the anode. Achieving this was very challenging, and required a significant design effort. Shielding saturation problems that were encountered in Phase 1 were resolved by increasing the shielding thickness and operating at a lower peak field. The HPA shielding consisted of three components. There were permendur flux shields at the top and bottom of the magnet bore which were external to HPA vacuum envelope. An iron anode with apertures was used to shape the beamlets, and was internal to vacuum envelope. Finally, iron inside the gun can was used to reduce the field between the cathode and anode as much as possible. The design activity was an iterative process that involved determining the field using MAXWELL, and then simulating the impact on the electron beamlets using MICHELLE. An example of a MAXWELL simulation of the axial field with shielding is shown in Figure 36. In this case small gaps (< 0.005 inches) in the external shielding around the electron gun were modeled. These gaps could not be avoided during the assembly of the tube. As shown in Figure 36, they led to significant leakage of axial field into the cathode region. Without the internal gun can iron shielding, this leakage field was 400 G. We were able to reduce this field to acceptable levels using this internal shield as well as external mu-metal shims.

Figure 37 shows one of two planar magnets fabricated by EEC for Phase 2. The bore is eight inches long, and the bore cross section is 1.4 x 4.5 inches. The magnet weighs about 80 lbs. Handles are provided for easier transport. The peak axial field is 6 kG, which is sufficient for good beam transmission through the circuit. Threaded bolt holes are provided at each end of the magnet to support the external shielding.



Figure 37 – Phase 2 planar magnet from EEC.

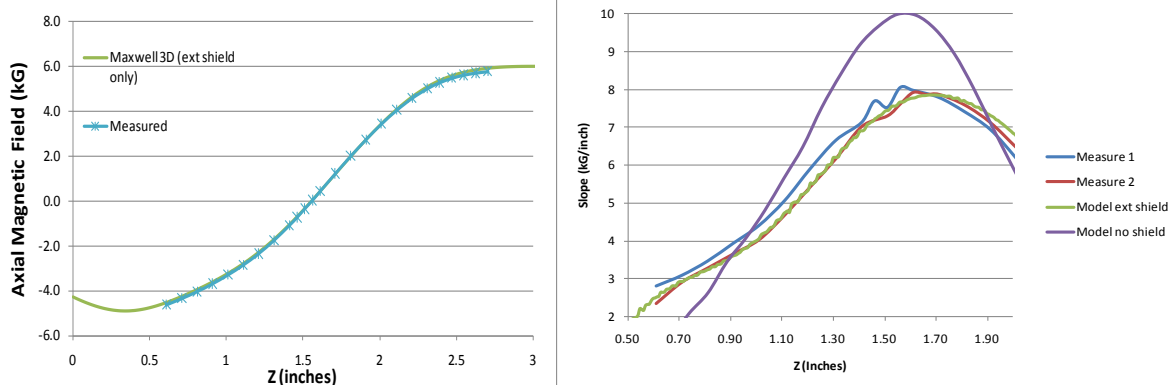


Figure 38 – Axial field of the first EEC planar magnet with external shielding installed.

The permendur external shielding was installed in the planar magnet bore, and axial field measurements were made. Results are shown in Figure 38. The axial field was found to be in good agreement with MAXWELL simulations. The graph on the left shows the axial field in the cathode region. The cathode is located approximately at the zero field location. The graph on the right provides another comparison. This figure shows that the reduction of the magnetic field gradient due to the external shielding agrees with the theoretical model. This indicates that the permendur B-H characterization used in MAXWELL is accurate. Further magnetic adjustments were made using shims after the tube was installed in the magnet. These shims were added during operation based on optimization of beam transmission through the FWG circuit.

### HPA Mechanical Layout

The mechanical layout of the 220 GHz HPA is shown in Figure 39. The design is a derivative of the HiFIVE beamstick, with the addition of an input and output port, and cooling channels for cw operation. The HPA was sized to fit in the larger bore EEC magnets built for Phase 2. The power-combined FWG circuit was cooled externally on the amplifier top and bottom with water jackets (darker blue component in Fig. 39). Thermal grease was used to provide good contact. The cooling channels in the jacket were designed to achieve the level of turbulence required for the assumed convection coefficient. A thermal analysis confirmed that the heat expected from electron beam interception would be properly dissipated and not lead to circuit damage. Standard WR-5 waveguides (in yellow) were used for input and output coupling through half-wavelength diamond windows. A vacuum pumping port was located at the gun end, and provided the vacuum conditions needed for space-charge limited emission. The single-stage collector was designed to minimize reflected electrons, and was more than 90% efficient based on MICHELLE simulations.

The test-stand layout for the HPA is shown in Figure 40. The EEC magnet sits on two XYZ translation stages to optimize electron beam transmission. Permendur shielding is permanently installed in the bore above and below the electron gun. The amplifier is held rigidly in place with mounting arms and supports. Because of the magnetic forc-

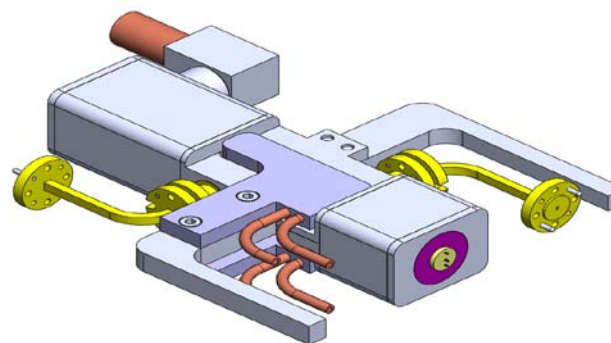


Figure 39 – HPA mechanical design

es associated with the iron shielding inside the gun can, a guiding installation fixture is required to gradually move the HPA into the proper position in the bore. WR-5.1 waveguide transmits the input RF power from a 220 GHz driver to a diamond input window and the output power to diagnostics. Two drivers were used: a 50 mW Virginia Diode, Inc., (VDI) multiplier chain amplifier and a Northrop Grumman Aerospace Systems (NGAS) source capable of 150 mW. In general we achieved the highest output powers with the NGAS source. Diagnostics that were used include RF Schottky detectors, and calorimeters made by Erickson, Scientech, and Keating.

### HPA Assembly

Sub-assemblies (collector, circuit carrier, etc.) were fabricated for Prototype 1 during the fall of 2011. Compatibility of the first diced FWG circuits from Teledyne with the carrier sub-assembly was verified. We also measured the beam tunnel dimensions, and found that the tunnel was deeper than expected. The design called for a  $220 \times 220 \mu\text{m}$  cross section, but instead we measured and found relatively large depth variations between 230 and 260  $\mu\text{m}$ . This deviation was probably due to the use of a new etching tool, and the dense FWG circuit pattern on the wafer. CHRISTINE simulations indicated that a small degradation in performance was expected because of reduced coupling impedance between the beam and RF wave. This could be partially offset by adjusting the HPA alignment so that the beamlets were closer to the circuit walls. However, a more serious consequence of this variation was an increase in the phase variation across the five circuits. As discussed earlier, this phase variation can cause a reduction in the combining efficiency by as much as 40-50%. Teledyne later fabricated a second set of DRIE circuits using double SOI wafers with two etch stops that controlled the depth of both the folded waveguides and the beam tunnels. Such a circuit was installed in Prototype 2.

Semicon successfully built the first HiFIVE cathode and shipped it to NGC in September, 2011. Figure 41 shows the cathode under test at Semicon, and Table 4 summarizes the temperature measurements. In order to reach 1100 °C, the heater must provide 19.5 W. This was consistent with our ANSYS thermal model of the cathode. There was also excellent temperature uniformity of the five emitters, with a small variation of 11 °C.

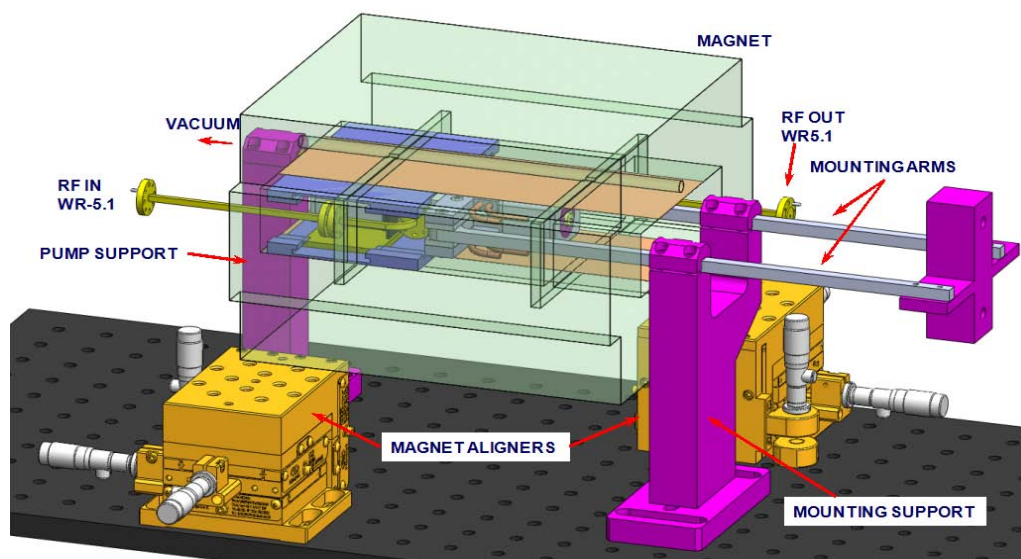


Figure 40 – HPA test-stand layout

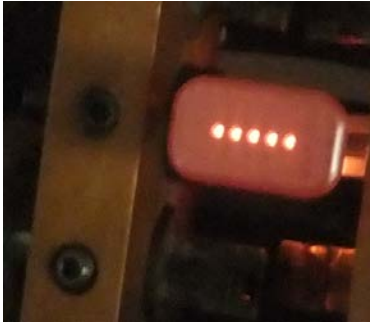


Figure 41 – Cathode tests

Table 4 – Cathode 1 Temperature Characteristics

Emitter	Ef [V]	If [A]	Tk [°C]
1	10.2	1.913	1095
2			1106
3			1098
4			1095
5			1100

We characterized the cathode emission in our bell jar. We operated the cathode up to about 15 kV, which is the voltage breakdown limit in our bell jar. The agreement with the theoretical curve was very good at lower voltages. The initial emission was a little low at the higher voltages, but improved with time. Operating at higher heater power allowed us to reach the design current of 200-250 mA at 19 kV. A second cathode was delivered by Semicon in October, 2011, and tested in our bell jar. The results are shown in Figure 42. In this case we operated at higher heater power, and were able to reach a space charge limited emission of 180 mA at 15 kV. We also ran at longer pulses in order to generate an image of the beamlets on a copper anode plate. The melt patterns produced by the five beamlets are shown in Fig. 43. As can be seen, there are actually fifteen melt spots. This is the result of the cathode slipping slightly in the support clamp during the tests due to vacuum pump vibration. We ended up with three sets of beamlet images. Each set exhibited good uniformity. The separation of the melt spots were within 0.03 mm of the design value (2.03 mm). Finally, the melt spot diameters of the lower images (obtained at higher current) were close to the prediction based on MICHELLE simulations (0.15 mm).

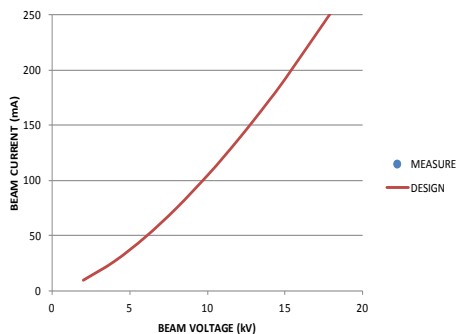


Figure 42 – Cathode 2 emission



Figure 43 – Melt images of the cathode beamlets

### Multi-Beam HPA Prototype 1

We completed the assembly of the first 220 GHz high power amplifier (HPA) prototype in December, 2011. The two biggest challenges were achieving satisfactory alignment, and welding a leak-tight tube. Alignment is more complicated for the HiFIVE HPA because three components are involved (cathode, iron anode, and beam tunnels). Normally, if the anode does not serve as a pole piece, then alignment is not as difficult. However, for the HiFIVE HPA, misalignment can

cause the beams to corkscrew in the circuits, increasing the risk of beam interception. Welding was challenging because of the large number of seams involved. After welding was completed, the HPA was processed up to 100 °C under vacuum on our exhaust station in order to achieve a low base pressure. We confirmed that the pressure was satisfactory for cathode emission, and was able to generate between 100-200 mA of beam current before installation in the magnet. This installation was difficult because of the strong magnetic forces on the iron anode and gun can shields. Special fixtures were used to ensure that the tube was installed correctly. The testing configuration is shown in Figure 44. A high voltage pulser provided 19 kV to the cathode. There was also a floating heater power supply that heated the cathode. The tube was held in place with two yokes, while the magnet position was adjusted to maximize transmission using two precision XYZ translation stages. The tube was water-cooled to remove excess heat resulting from the dispenser cathode and from beam interception.

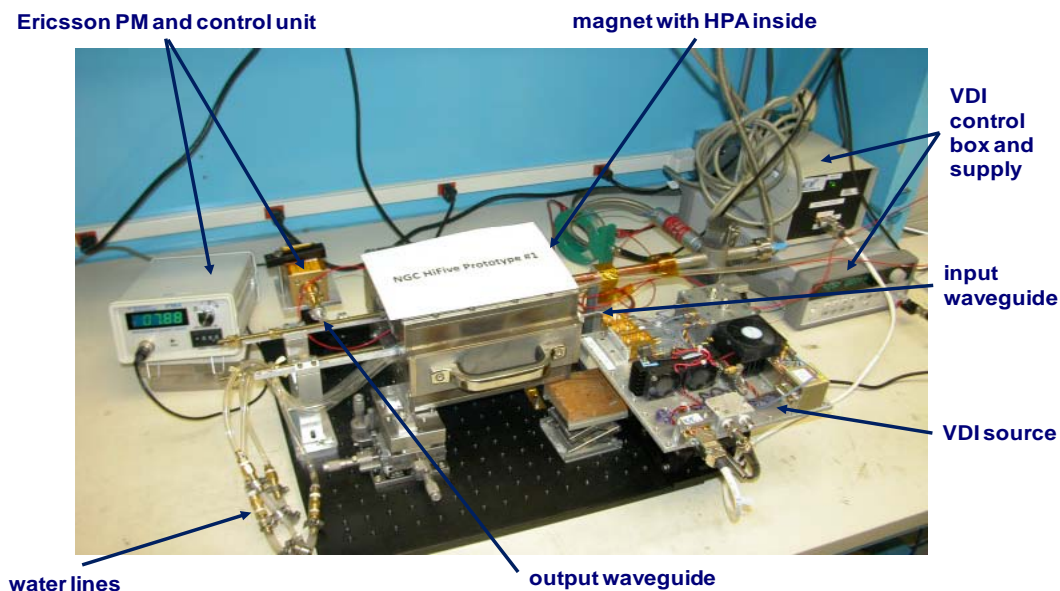


Figure 44 – Testing of the first HPA prototype

Initial testing of Prototype 1 achieved 19 kV and 135 mA of current with 25% beam transmission to the collector. Unfortunately the cathode heater failed at this point. X-ray imaging indicated that the wire leading to the cathode coil overheated, leading to a break. This was an unusual failure, but proved to be a recurring problem with the HiFIVE cathodes. We determined that we could replace the electron gun and rebuild the HPA. The tube was successfully rebuilt and processed. After emission was confirmed, the tube was pinched-off and installed in the magnet. Then the VDI driver was attached and diagnostics were prepared for power measurements and RF pulse characterization. We achieved a low HPA base vacuum pressure, indicating that the input and output diamond windows were tight. After careful cathode processing, we reached the design current of 250 mA at 19 kV. The measured emission is shown in Figure 45. The dots are measurements, while the solid line is the prediction based on space charge emission. The data was in reasonable agreement with theory, suggesting that the five emitters were operating close to the space charge limit and therefore providing similar currents to each of the FWG circuits. However, there is a small discrepancy between the data and theory, suggesting that the five emitters do not have identical emission characteristics.

We continued to improve the beam transmission, and by late March, 2012, had achieved up to 61%. The results are given in Figure 46. The graph shows how transmission increased as we operated closer to the design current, which corresponds to optimum focusing. In addition to operating closer to the design point, we also tried using shims to reduce the transverse error fields. When we reached our goal of 30 mA per circuit for Prototype 1, we began short pulse RF testing (20  $\mu$ s, 0.33 Hz). Using the Erickson calorimeter, we detected RF when operating at 219.3 GHz (the highest input drive provided by our VDI source). We initially measured peak powers up to 10 W.

We continued to optimize performance and utilized two drivers: our lower power VDI source and the higher power source from NGAS. Table 5 summarizes our short pulse test results for Prototype 1. Using the VDI source, we reached 20.4 W at the window at 220 GHz, and 34 W

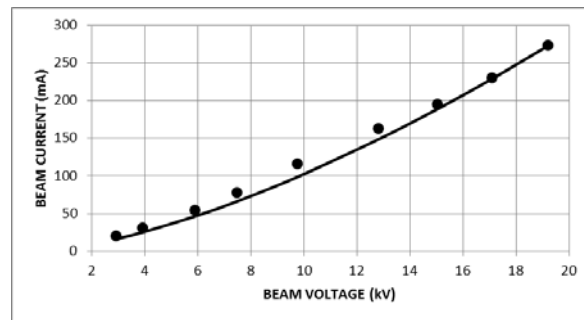


Figure 45 – Prototype 1 cathode emission

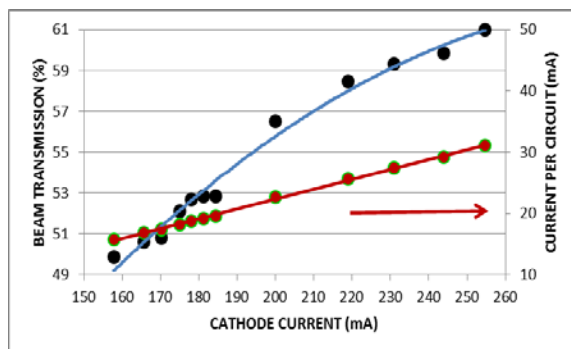


Figure 46– Transmission efficiency (blue) and current per circuit (red)

Table 5 – Prototype 1 Test Results

	UNIT	GOAL	HPA PROTOTYPE 1					
Drive source			VDI	VDI	NGAS	NGAS	NGAS	NGAS
Frequency	GHz	220	220.2	217.3	219.3	214.0	214.0	213.4
Beam voltage	kV	19.1	19.1	19.4	19.2	19.8	19.8	20.0
Cathode current	mA	250	242	248	266	277	264	268
Transmitted current	mA	175	146	148	160	163	181	202
Transmission	%	70	60	60	60	59	69	75
Drive power	mW	100	59	55	115	135	146	146
- at window	mW	63	39	37	67	79	85	85
- at FWG circuit	mW	43	26	24	44	51	55	55
Output power at circuit	W	50	20.4	34.0	38.9	72.5	59.8	70.8
Output power at window	W	40	16.1	26.6	30.5	55.5	45.8	54.2
Circuit efficiency	%	1.5	0.73	1.19	1.26	2.25	1.67	1.76
Collector efficiency	%	85			94%	94%	94%	94%
HPA efficiency	%	2.1			1.4%	2.3%	2.5%	3.4%
Gain - HPA	dB	26.0	24.4	26.8	26.6	28.5	27.3	28.0
- Combined Circuit	dB		28.9	31.5	29.4	31.6	30.4	31.1
- Individual Circuit	dB		31.4	34.0	31.9	34.0	32.8	33.6
Bandwidth	W-GHz	200			158.2	246.8		

at 217 GHz where the gain is higher. It was clear that we were not saturating the HPA, so we switched to the NGAS source, which produces a maximum of 165 mW compared to the VDI source maximum of 55 mW. As a result of higher drive, we reached 30.5 W at 219.3 GHz, and 55.5 W at 214 GHz. We were able to demonstrate all the HiFIVE metrics except HPA efficiency, although not simultaneously and only for short pulses. We needed to improve transmission to 85-90% in order to meet the efficiency metric and to operate at higher duty. The calculated power at the FWG circuit in Table 5 was determined by taking into account window and output waveguide losses. At 214 GHz the calculated FWG power was 72.5 W. If we assumed a FWG combining efficiency of about 60%, then the total power of the five FWG circuits before the combiner could exceed 100 W at 214 GHz. In addition to maximizing output power, we also ran with a depressed collector at 219 GHz, and demonstrated 94% collector efficiency. Figure 47 shows Prototype 1 scope traces for voltage (blue), cathode current (red), collector current (yellow) and RF (green) during short pulse operation. For this case, the cathode current is 267 mA, of which 181 mA reaches the collector for a transmission efficiency of 68%.

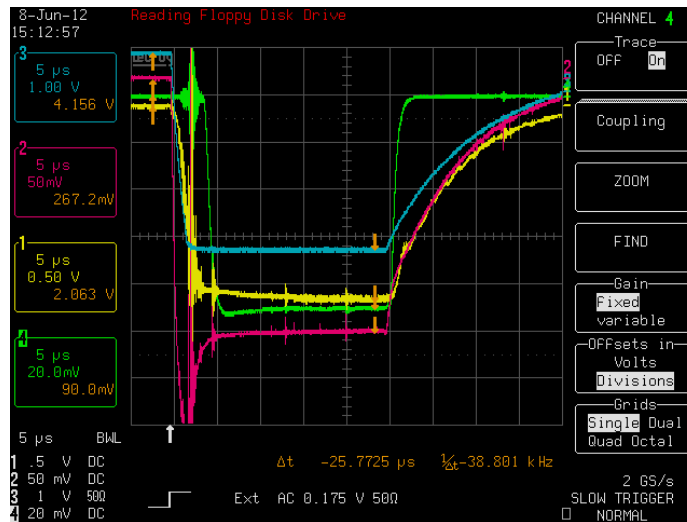


Figure 47 – Prototype 1 pulse traces

In order to operate the HPA at higher duty and avoid damaging the FWG circuit, we needed to increase the beam transmission to 85-90%. To reach this transmission goal, we implemented HPA test-stand improvements to reduce magnetic field errors and improve the tube alignment. We rebuilt the alignment fixtures used to position the magnet to provide more flexibility, optimized the position of the planar magnet, and used shims to reduce the magnetic field errors. We also operated with the second planar magnet built by EEC. Measurements of the magnetic fields in the bore indicated that this magnet had smaller transverse error fields. We also increased the amount of external permendur shielding in the gun region. The biggest improvement occurred when additional mu-metal shielding was inserted above and below the electron gun. This suggests that the field in the cathode-anode region was higher than expected and causing distortion and deflection of the beamlets. At the end of the optimization phase we reached 75% current transmission to the collector.

Typical RF results from this testing phase are shown in the last two columns of Table 5. The window RF power at 214 GHz was lower than before (46 vs 55 W). We believe that the lower

power may be due to the fact that the electron beam is more centered in the beam tunnel and therefore coupling between the beam and RF is slightly lower. However, we did find a better operating point at 213.4 GHz, and as a result were able to simultaneously achieve good beam transmission (75%) and high power at the window (54 W). This resulted in our best HPA efficiency (3.4%) based on a collector efficiency of 94%.

We attempted to run at a higher duty cycle by increasing the pulse width and repetition rate. Our goal was to reach a duty cycle of 1%. The collector was depressed by 90% in order to reduce the dissipated power. We were able to operate at 1 Hz with 10 ms pulses (1% duty). RF measurements indicated that the circuit was operating as expected, and no damage was occurring. Unfortunately we experienced another cathode failure, and this ended testing of Prototype 1.

### Multi-Beam HPA Prototype 2

The second HPA prototype was built with a DRIE circuit fabricated using a double SOI wafer. The carrier was assembled with the FWG circuit and diamond vacuum windows, and cold test measurements were completed at NGAS using their 220 GHz network analyzer. The results are shown in Figure 48. Shims were used to optimize the match between the external WR-5 waveguide and the diamond window disks. This resulted in an input port match of 2:1 (9dB) or better from 210-230 GHz, and 1.4:1 (15.5dB) or better from 214-226 GHz. The output port match was 2:1 (9dB) or better from 212-227 GHz, and 1.6:1 (13dB) or better from 217-226 GHz.

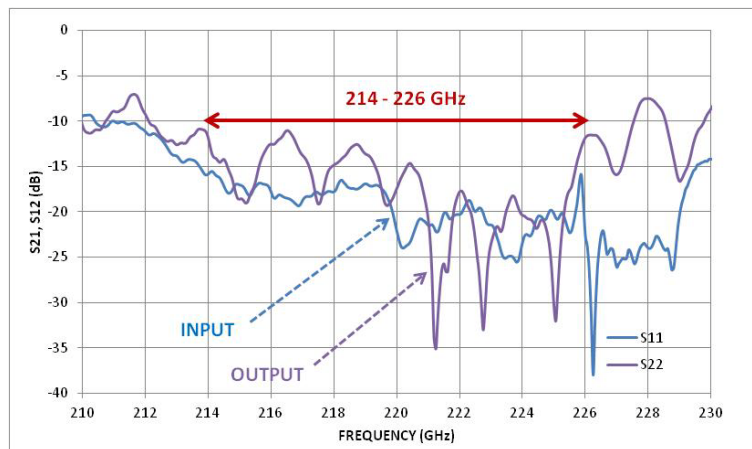


Figure 48 – Prototype 2 cold tests

This prototype also used an internal permendur gun shield rather than an iron shield. It was hoped that the better shielding provided by the permendur would result in improved beamlet formation and transmission. However, only 15-20% of the beam reached the collector. We ultimately determined that the anode had tilted and was deflecting the beamlets before they reached the circuit. It was likely that heat from the cathode had caused the anode plate to expand and break support welds along one edge. We repaired the anode and conducted a second round of testing with Prototype 2. The best RF performance was poor compared to the results achieved with Prototype 1. We eventually stopped tests and opened the HPA to examine the DRIE circuit. The RF splitter at the beginning of the DRIE circuit had been significantly damaged during initial testing while the anode was tilted. As a result little drive power was reaching the FWGs. At this point we focused our attention on HiFIVE Prototype 3.

## 5.0 PHASE 3 TECHNICAL RESULTS

### Multi-Beam HPA Prototype 3

A third prototype was built and tested during 2013. The cathode was activated in our bell jar and operated up to 5 kV to verify emission. The results are shown in Figure 49. The emission closely followed the space charge design limit, and matched the performance of the first prototype. We carefully inspected tube welds to ensure that they were robust. In particular, we strengthened the iron anode so that it did not tilt due to magnetic forces. Assembly, processing, and activation were completed in March, 2013. The tube was then potted to allow operation at higher voltages, and installed in the planar magnet. A photo of the experimental setup is shown in Figure 50.



Figure 49 – Prototype 3 cathode

Figure 50 – Prototype 3 testing

The goal of initial testing was to achieve the design current and optimize transmission. Operation at 20 kV was demonstrated, and a maximum cathode emission of 247 mA was measured after a week of operation. This is close to design value of 250 mA. A beam transmission through the FWG circuit of 34% was obtained after using magnetic shims in the gun region. This is lower than the transmission achieved with both Prototype 1 and 2 ( $> 50\%$ ). At this point, in an attempt to improve performance, the tube was rotated 180 degrees and realigned in the magnet. This was a better configuration. Preliminary optimization achieved 48% transmission at 18.5 kV, with 109 mA reaching the collector. This is comparable to the initial performance of the earlier prototypes. We were in the process of further improving beam propagation when we experienced another cathode failure. The heater wire opened, most likely due to thermal stress associated with the high power (22 W) required to achieve the emission temperature. As with earlier cathodes, it is likely that the gun heater package was operating very close to its thermal limit.

The tube was extracted from the magnet, and rebuilt with our last five-beam cathode. Our goal was to keep the cathode heater power below 20 W to reduce the thermal stress and increase life-time. This increased the time required to achieve the design beam current (250 mA). Before building the tube, we imaged the beam with a copper foil in our bell jar and found the cathode and anode holes aligned to within two mils. The rebuilt HPA prototype was successfully processed and installed in the planar magnet. We began operating again in June, 2013, with 20  $\mu$ s pulses at 1-3 Hz. The beam transmission was maximized by optimizing the magnet position and placing shims in the gun region. We reached 191 mA of emission at 19 kV. The highest collector

current was 129.6 mA, corresponding to a transmission efficiency of 70.9%. This is comparable to our best results with Prototype 1.

The rebuilt HPA prototype was operated with short pulses for a month. Both the VDI and NGAS sources were used as drivers. Results are shown in Table 6. Beam transmission typically was between 60-75%, with the better results occurring at higher currents where the beam optics was optimized. The highest transmission efficiency was 78%, which was close to our goal of 80%. The best RF results were achieved with the VDI source, even though it provided less drive power than the NGAS source. The VDI driver provided better shot-to-shot stability, which made performance optimization easier. The highest power was achieved at 210.2 GHz, which is well below the design frequency of 220 GHz. We believe this was the result of a waveguide depth that is greater than the design value of 762 microns. We measured other FWG circuits from the same fabrication set and verified this. The highest RF power at the output window that we measured was 34.8 W, which corresponds to a circuit efficiency of 1.95%. The corresponding HPA gain was 33 dB. This result was achieved at a relatively low transmitted current of 125 mA. We continued to increase the transmitted beam current towards the 200 mA design value, with the goal of achieving transmission greater than 80%. This higher transmission would allow us to increase the duty cycle to 1-10%. Unfortunately, in spite of carefully operating the cathode heater below 20 W, we experienced another failure, which effectively ended our testing of multi-beam HPAs.

Table 6 –HPA Prototype 3 Experimental Results

	UNIT	PROTO 3		
		VDI	VDI	NGAS
Drive source				
Frequency	GHz	216.1	210.2	210.2
Beam voltage	kV	17.9	18.7	18.4
Cathode current	mA	184	192	197
Transmitted current	mA	110	125	153
Transmission	%	60	65	78
Drive power	mW	45	30	140
- at window	mW	26	18	82
- at FWG circuit	mW	17	11	52
Output power at circuit	W	22.6	45.5	34.2
Output power at window	W	17.3	34.8	26.2
Circuit efficiency	%	1.15	1.95	1.21
Gain - HPA	dB	28.2	33.0	25.1
- Individual Circuit	dB	33.7	38.5	30.6

### Single-Beam Amplifier

The second goal of Phase 3 was to design, fabricate, and test a higher-duty single-beam amplifier. This was a return to a more traditional VE geometry, and made the overall HPA fabrication easier. A single-beam device is mechanically simpler, and eliminates the need for a power splitter and combiner as part of the RF circuit. In addition, a compact symmetric radial access magnet can be used to propagate the beam. Because of the single beam, no magnetic elements were required in the tube, making magnetic alignment significantly easier.

The design parameters of our 50 W HPA are listed in Table 7. The design was based on requirements for the DARPA Visual SAR (ViSAR) program. The amplifier operates at 19.52 kV with 95 mA of beam current. CHRISTINE simulations predict that RF powers in excess of 62 W could be generated at the FWG circuit output over a 231.5 – 235.0 GHz bandwidth. Taking into account RF attenuation from the circuit output to the diamond vacuum window, the expected HPA peak power exceeds 50 W over the desired bandwidth. However, the drive power is significant, especially at the band edges. The requirements for the HPA single-beam electron gun are less challenging compared to the multi-beam gun. The current density is 17 A/cm<sup>2</sup>, and only 6 W of heater power is required to achieve good emission, compared to the 20 W needed by the five-beam cathode. So the risk of a cathode failure was small. Figure 51 is a MICHELLE simulation of the beam propagation through the FWG circuit. Under ideal conditions transmission is expected to exceed 99%. In reality magnetic field errors and misalignment were expected to lower transmission to about 90-95%. Edge emission from the cathode is a significant concern, and we incorporated a biased focus electrode to reduce this emission. Although the center frequency of a ViSAR system is 233 GHz, we chose to operate at 220 GHz because of the availability of high power drivers as well as calibrated diagnostics at our test facilities.

Table 7 – 233 GHz Amplifier Design

CHRISTINE 1D SIMULATIONS			
Parameter	Value		
Beam Tunnel	280 x 280 $\mu\text{m}^2$		
Beam Radius	105 $\mu\text{m}$		
Beam Fill	75%		
Beam Voltage	19.52 kV		
Beam Current	95 mA		
Circuit Length	3.2 cm		
Frequency	231.5 GHz	233.0 GHz	235.0 GHz
Pmax @ circuit	64 W	75 W†	62 W
Gain @ Pmax	23.6 dB	27.8 dB	21.5 dB
Gain, SS	30.4 dB	32.7 dB	19.6 dB
Pin for 62 W output	201 mW	51 mW	379 mW
Source drive	358 mW	91 mW	674 mW

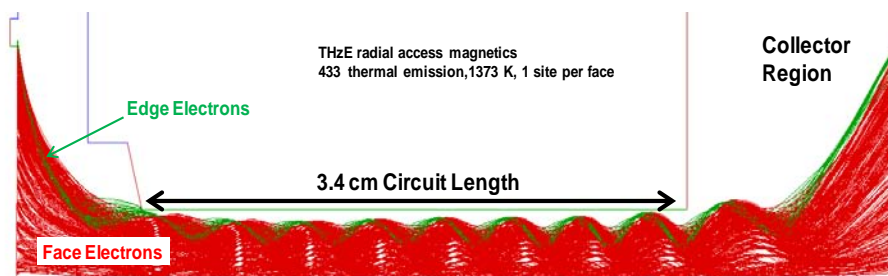


Figure 51 – Electron beam MICHELLE simulations

In addition to optimizing the beam optics with MICHELLE, achieving high beam transmission through the FWG circuit also required careful assembly of the tube. First, accurate location of the focus electrode relative to the cathode was necessary. This was achieved through precision fixturing. This took into account the 0.0005 inch of thermal expansion of the cathode assembly that occurs when operating at high temperatures. Accurate placement of the focus electrode is required to ensure that the emission of electrons from the edge of the cathode is minimized. These electrons typically experience significant scalloping and intercept the walls of the FWG circuit, increasing the thermal load. Second, the true beam position at the gun exit was determined prior to tube assembly by creating a melt spot on a small copper foil attached to the anode during bell-jar emission testing. This spot was used to center an alignment ring that was attached to the gun. Another ring was welded to the circuit-carrier assembly and centered on the beam tunnel of the RF circuit. The alignment process was completed by mating these two rings during final assembly of the tube. This fabrication approach reduced the offset of the electron beam and circuit to less than 0.001 inch.

The goal of the single-beam HPA was to generate 50 W of peak power, and to operate at a duty cycle of 5-10%. In order to understand the thermal implications, we simulated the temperature and thermal stress of the FWG circuit using ANSYS. Figure 52 is an example of the effect of beam interception along the folded waveguide. We assumed 20 W of average heat deposited on five bends. In this case we recessed the posts so that they were protected from impinging electrons. We assumed that beam scraping is greatest at the center of the RF circuit, with a deposited peak thermal load of 76 kW/cm<sup>2</sup>. Water cooling behind the circuit was used to remove the heat. ANSYS predicted a peak temperature of 500 - 600 °C along the edge of the beam tunnel. This is quite high, but below the melting temperature of silicon (1414 °C). The reason for the high temperature is the lower thermal conductivity of silicon compared to metals such as copper. Stresses were below 1 GPa, which is also high but acceptable. There was also concern that pulsing the amplifier would lead to cyclic fatigue. It was hoped that careful fabrication of the tube would reduce beam interception and lower the wall temperature. Another option that we investigated was the deposition of a thicker copper metallization on the silicon substrate. A thicker layer would dissipate the heat due to beam interception more effectively, and reduce the wall temperature to 400 - 500 °C. Past FWG circuits had a copper layer thickness of about 2-4 microns. Our goal for future single-beam HPAs is to increase this layer to ten microns.

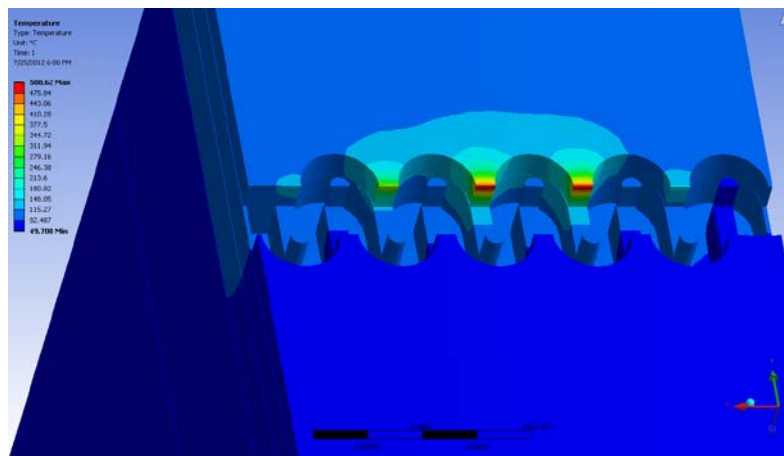


Figure 52 – ANSYS thermal modeling of FWG circuit

We completed a mechanical layout of the single-beam HPA during Phase 3. The layout is shown in Figure 53. The design is based on a radial access magnet. Input and output transmission waveguides access the RF circuit through a central gap. This reduces the power requirements for the RF driver and increases the delivered output power. The RF circuit is centered in the magnet in a field of about 7 kG. A single-stage collector consisting of a long pipe is used to recover the energy of the spent beam. Figure 54 shows the electron trajectories in the collector. As the electrons propagate away from the magnet, the field decreases and the electron beam expands and intercepts the side walls. This expansion reduces the wall power density. About 80 watts of heat is dissipated in the collector. Power is dissipated uniformly on the ID of the pipe between 1 and 2 inches from the end. The power density is 39.5 W/cm<sup>2</sup>. Based on this thermal load, a graphite collector would reach 374°C, while a copper collector would reach 187°C. While graphite does reach a higher temperature, it is preferable because it emits fewer secondary electrons that could propagate back towards the gun and disrupt operation.

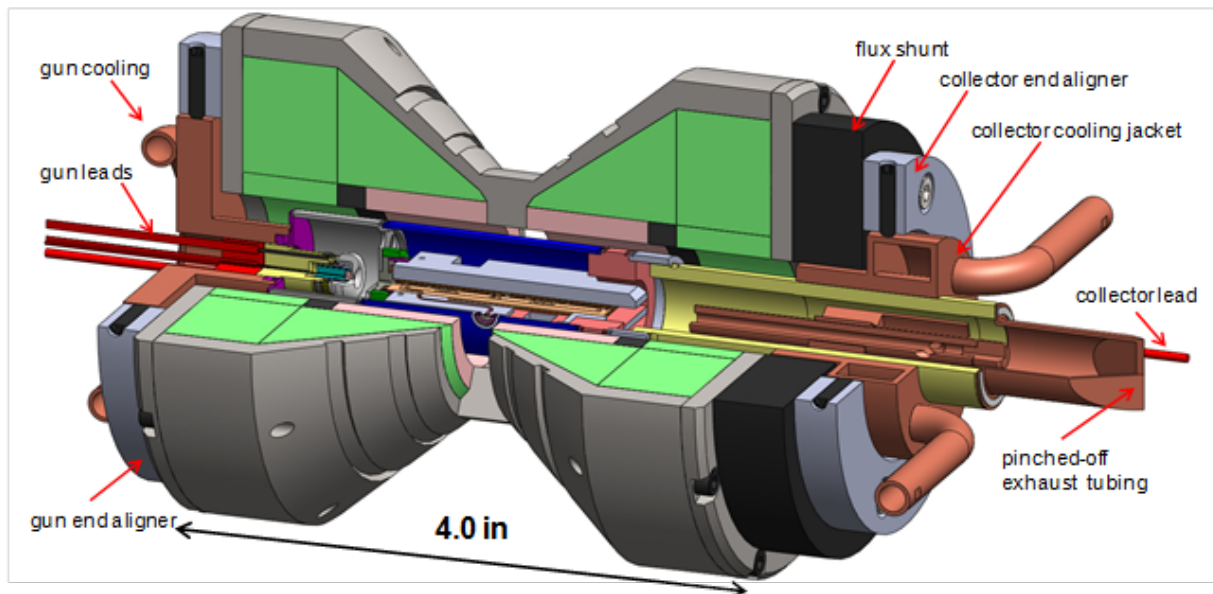


Figure 53 – Amplifier mechanical layout

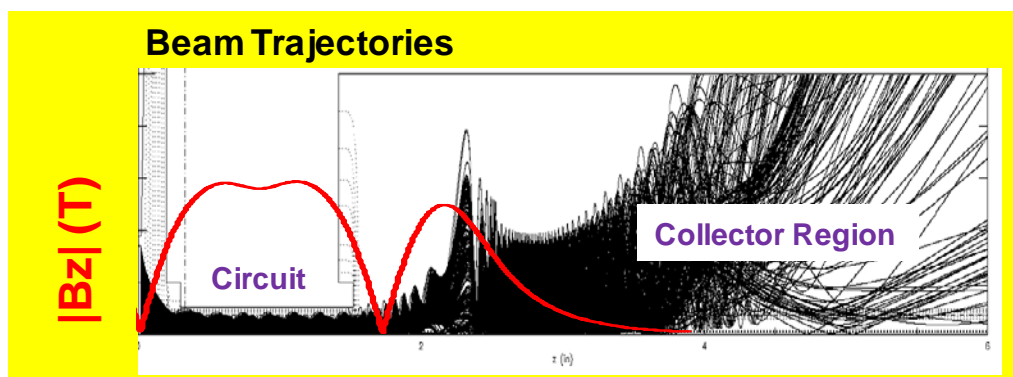


Figure 54 – Electron trajectories from the gun to the collector

We completed MICHELLE simulations of the electron beam to determine the amount of beam interception in the FWG circuit. The beam envelope is shown in Figure 55. The gun is located at the left, and the red curve represents the circuit beam tunnel radius with a radius of 130  $\mu\text{m}$ . MICHELLE predicts about 99% transmission for an ideal beam. The measured transverse magnetic field errors (about 20 G) will cause additional beam loss due to deflection. Prototype 3 had a copper beam scraper before the RF circuit to eliminate the cathode edge emission most likely to intercept the FWG circuit. Our goal for Prototype 3 was to achieve greater than 90% transmission to the collector.

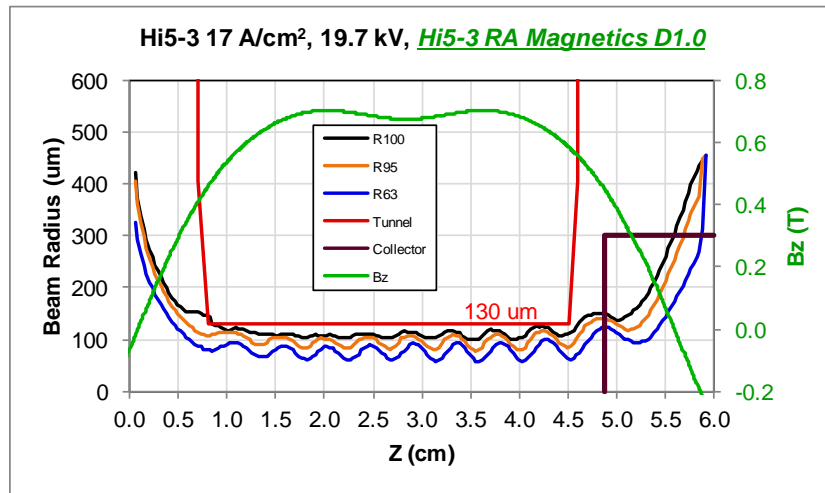


Figure 55 – Beam envelope based on MICHELLE simulations

The HPA used a radial-access magnet (see Figure 53) to guide the single beam. Input and output transmission waveguides accessed the FWG circuit through central gaps in the magnet casing. This reduced the waveguide lengths, lowering the ohmic attenuation. As a result, less RF driver was required and more output power was delivered. The FWG circuit was centered in the 7 kG magnetic field. The first radial-access magnet is shown in Figure 56. The transverse field was measured, and the expected beam envelope was calculated. Results are shown in Figure 57. The left graph indicates that the maximum transverse field is about 16 G and is located in the cathode region (0 cm). The right curve is a plot of the beam envelope (blue) and the radial position of the FWG circuit wall (blue). The beam does get close to the circuit wall due to deflection by the transverse magnetic field, but minimal scraping is predicted.

EEC delivered two additional magnets using different processes for further reduction of transverse error field. In the second magnet the two end rings were independently rotated while measuring the transverse field. This resulted in only slightly reduced transverse error field in the completed second magnet. A far more effective approach was applied for the third magnet, where the two rings and the two conical end sections were all independently rotated. This technique resulted in a reduction of the measured transverse error fields by a factor of four.

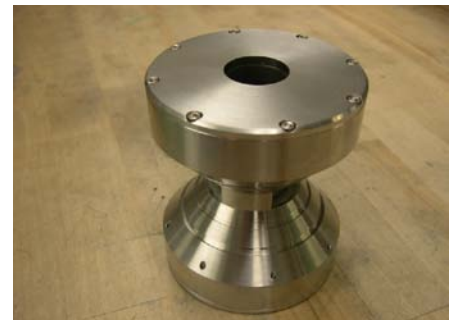


Figure 56 – Radial access magnet

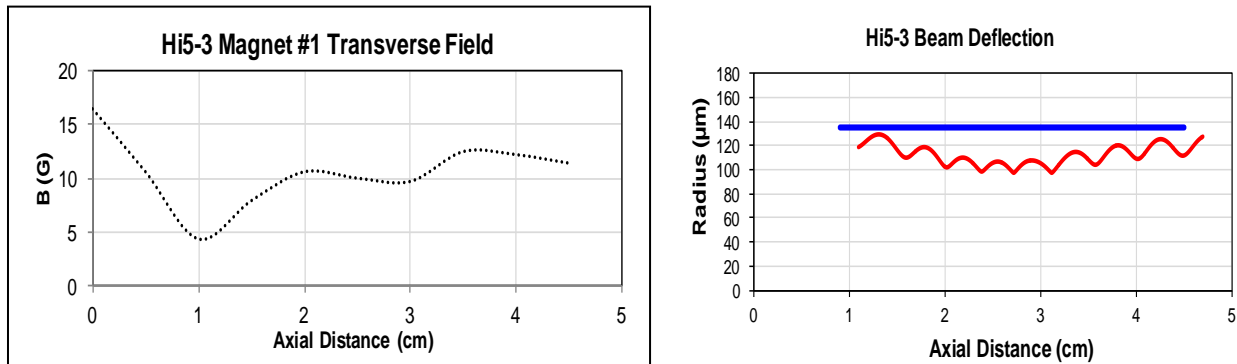


Figure 57 – Measured transverse fields (left) and calculated beam envelope (right).

HPA tube parts were ordered from Custom Microwave and arrived in June, 2013. The DRIE circuits from TSI also arrived at that time. An electron gun was assembled and emission tests were conducted. A beam image was made on a copper foil at the anode aperture, and measurements indicated that the beam was aligned to the anode center to within 0.001 inches. The TSI circuits were characterized to determine if they met dimensional specifications. The beam tunnels were found to be substantially deeper than the design value of 290  $\mu\text{m}$ . These circuits were made from single SOI wafers, so only the waveguide depth was controlled by an etch stop. We had decided to use a single SOI wafer because phase control was not as critical for a single-beam HPA, and the second etch layer results in a higher bonding temperature. This higher temperature was associated with the degradation of circuit quality in earlier circuit fabrications. We simulated the effect of the larger beam tunnels on the coupling between the electron beam and RF wave. A CHRISTINE analysis of coupling was completed that indicated that an output RF power of about 50 W could still be achieved if we operated closer to cutoff, but the bandwidth would be slightly reduced. Operating closer to cutoff would require a higher beam voltage (20.3 kV). Teledyne subsequently reviewed their etching processes to determine the cause of the larger beam tunnel. We concluded that double SOI wafers should be used in HPAs to control both the waveguide and beam tunnel depths, even though the wafer bonding process becomes more complicated.

The tube was installed in the radial-access magnet and short pulse RF testing was started. The test stand is shown in Figure 58, and operating results are given in Table 8. Cathode emission close to the design value (107 mA) was obtained, indicating a good tube base pressure. Excellent beam transmission was achieved, with 95-99% of the beam reaching the collector. Alignment was relatively easy because of the large beam tunnel. An output power of 19.4 W was measured at 212.2 GHz using the VDI source as the driver. It is likely that the tube was under-driven because the VDI source generates less than 30 mW at 212.2 GHz. No spurious oscillations were detected.

The HPA generated the highest power at 212 GHz, well below the design point of 220 GHz. Figure 59 shows the frequency versus beam voltage for maximum power. For 220 GHz operation, the optimum voltage was 17.6 kV instead

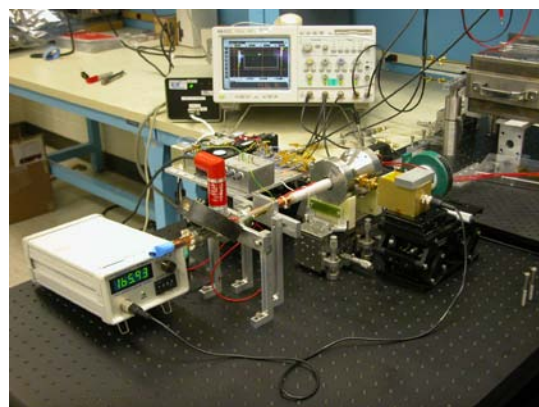


Figure 58 – Single beam HPA under test

of 19.7 kV. This data suggests that the waveguide depth is larger than desired. In order to verify this, another FWG circuit made during the same fabrication cycle was analyzed. The distance between the etch stops on the full die was measured and used to determine the waveguide depth. The depths along the circuit averaged 778  $\mu\text{m}$ , well above the design value of 762  $\mu\text{m}$ . If the optimum design point is adjusted to reflect this larger waveguide depth, then there is better agreement with our simulations. We also measured a large depth variation along the circuit, which causes a de-phasing of the electron beam and RF wave. This probably explains the lower power that we measured. The depth variation indicates a possible problem with the wafer bonding process that will need to be addressed in future HPAs.

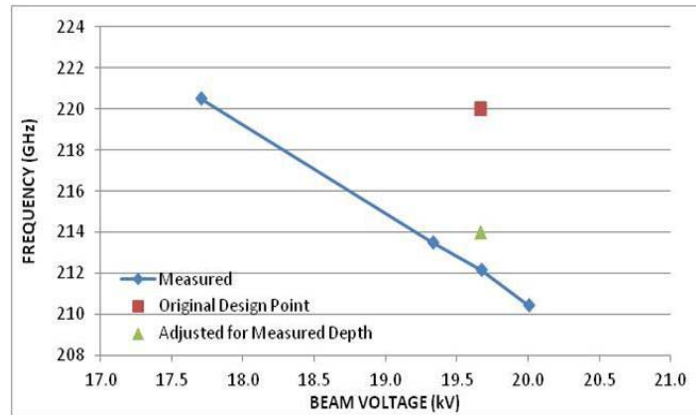


Figure 59 – Operating frequency versus beam voltage

After short pulse testing was completed, we attempted to increase the duty cycle to 1 – 5%. We operated with 30  $\mu\text{s}$  pulses, and increased the duty cycle up to 1 kHz. These tests gave us a sense of the robustness of the FWG circuit. We monitored the RF output for variations that would indicate that the FWG circuit was being damaged by the beam. Our goal was to reach a duty cycle of 3-5%. Our thermal model of the FWG circuit indicated that, for this duty, the peak temperature on the circuit wall due to beam interception would be between 250 and 300  $^{\circ}\text{C}$ . Our duty was limited because no water cooling was incorporated directly into the HPA, and the tube was baked at relatively low temperatures ( $\sim 100^{\circ}\text{C}$ ). We did use air-cooling on the collector and through the radial access gap in the magnet. We were able to operate at 3.2% duty at the end of tests. The current through the circuit was 100 - 110 mA, with 95% beam transmission. The measured RF peak power remained relatively constant at about 15 W throughout testing, indicating that the DRIE circuit was not being damaged by the beam.

Table 8 – Single Beam HPA Test Results

Parameter	Design Value	Test Value
Center Frequency	220.0 GHz	212.2 GHz
Current	107.0 mA	106.7 mA
Voltage	19.7 kV	19.7 kV
Emission Density	17.0 A/cm <sup>2</sup>	17.3 A/cm <sup>2</sup>
Transmission	99.8%	97.8%
Heater Power	$\leq 6$ W	4.6 W
Power at Window	63.0 W	19.4 W
SS Gain	31.2 dB	32.4 dB

---

## 6.0 FINDINGS AND CONCLUSIONS

The HiFIVE program at NGES resulted in the successful demonstration of high power amplifiers at frequencies between 210 and 220 GHz. Two configurations were investigated: A multi-beam amplifier in a planar magnet and a single-beam device in a cylindrical magnet with radial access. An important aspect of this program was the successful use of precision DRIE micro-fabrication techniques to achieve the stringent specifications for the folded waveguide circuit dimensions and tolerances. Our best test results can be found in Tables 5 and 7. In the case of the five-beam HPA, peak output powers up to 31 W were measured at 219 GHz. Even higher powers (55 W) were produced at 214 GHz because of the higher gain at lower frequencies. A power-bandwidth of 247 W-GHz was measured at 214 GHz, and the overall gain was 28.5 dB. The single-beam HPA generated 19.4 W at 212 GHz. We were able to operate this device at a 3.2% duty cycle without damaging the FWG circuit. We also achieved good beam transmission efficiency through the FWG circuit in both devices. For the multi-beam HPA, up to 75% of the beam was transmitted through the RF circuit to the collector. The single-beam HPA had even better results, with a transmission efficiency as high as 99%.

Successful development of HPA sub-components was critical to our HiFIVE program. In particular, the cathodes, FWG circuits, and magnets required considerable attention. The following sections will summarize the challenges, and the lessons that were learned, during the development of our multi-beam and single-beam HPAs.

### Multi-Beam HPA Development

#### FWG Circuit Design

- The Phase 1 of HiFIVE required the demonstration of a beamstick with an aspect ratio of 25. This requirement was based on an NRL design study of a 220 GHz amplifier. We found that this conclusion was highly dependent on the initial HPA assumptions, such as the amount of beam intercept and the maximum FWG temperature. Our analysis concluded that a five-beam configuration would provide most of the thermal benefit of a high aspect ratio HPA, and would meet the HiFIVE requirements. A five-beam HPA was also much easier to build.
- Our analysis indicated that operating at higher voltage and lower current was optimum and would reduce the amount of beam interception in the FWG circuit. But higher voltage increases the size of the gun and magnet because of voltage breakdown limitations. We chose 20 kV as a compromise between these two effects.
- The circuit beam tunnel was made as large as possible while maintaining good coupling between the electron beam and RF wave. This led to better beam transmission efficiency. However, a large tunnel causes reflections at the periodic crossings between the FWG and beam tunnel. This causes resonances that result in reflected power, a complex RF output spectrum, and possible spurious oscillations. The best way to avoid this problem is to increase the beam current density, and thus reduce the size of the beam and the tunnel.

#### FWG Circuit

- Our HPA results indicated micro-fabrication technology can meet the dimensional and tolerance requirements of a 220 GHz FWG circuit. Our proposed approach, which consisted of

two halves that were aligned and bonded, gave very good results. Alignment of the two halves to within 2-4  $\mu\text{m}$  was achieved using well-established optical techniques.

- Controlling the depth of both the waveguide and the beam tunnel along the entire circuit is critical to achieving high efficiency. This is required to maintain the proper phase between the electron beam and RF wave. Our original circuits were made from simple silicon circuits, but depth control was difficult. We eventually introduced silicon dioxide layers (SOI and DSOI) that served as etch-stops and provided the required dimensional accuracy. The disadvantage of these layers is their poor thermal conductivity. They increased the temperature required for bonding, which occasionally caused de-lamination of copper layer deposited on the walls. Careful process development minimized this problem, but did not eliminate it.
- The copper electroplating process was initially started with a gold seeding layer using a TSI deposition tool. But the gold resulted in some quality problems, especially at higher bonding temperatures. TSI eventually switched to a copper seed layer deposited by an external vendor. This change improved both the quality and yield.
- Our RF power combiner and splitter geometry worked well, and resulted in the desired electrical length for all the circuits. The disadvantage of our configuration was the possibility of a spurious oscillation in one of the FWG circuits. This is due to the strong reflection that occurs at either the splitter or combiner when only one circuit is excited. In order to avoid this, the sever must be carefully designed with sufficient attenuation to prevent oscillations.

#### Planar Magnet

- We decided to use a planar magnet with a field (7-9 kG) well above the minimum requirement based on Brillouin flow. We felt this would provide us with better control of the beam with less scalloping, which would reduce beam interception in the FWG circuit. However, the magnetic shielding required for proper beamlet formation became more difficult at high field. The shields were prone to saturation, resulting in the need for thicker shields made of permendur. This required a larger magnet bore, increasing both the size and weight of the HPA module. In later designs the magnetic field was reduced, and beam optics became easier. This was an important factor that allowed us to achieve 75% transmission.
- Another factor that affected the magnet size was the need for low transverse field errors at the beamlets that would cause deflection. The lowest risk approach was to make the bore sufficiently large that the beamlets were positioned far from the magnet bore walls. We made the beamlet array as small as possible based on fabrication limitations. The final design still resulted in a relatively large magnet weighing eighty pounds.
- Another tactic that was used by EEC to reduce field errors was to fabricate the magnet so that the seams between the Nd-Fe-B segments were not close to the electron beamlets. The magnet segments are epoxied together, and small gaps and misalignments can occur. If these fabrication errors are not close to the beamlets, then better beam transmission is possible.
- To properly form the electron beamlets that propagate through the circuit requires magnetic shielding and an iron anode. This results in significant forces on the tube when it is installed in the magnet bore. This installation process, as well as precisely aligning the tube to optimize transmission, required precision fixturing that needed to be carefully designed and fabricated. This was a challenging task for us that required a number of iterations before we found a satisfactory approach.

---

## Electron Gun

- We evaluated different technologies during HiFIVE Phase 1, including carbon nanotube cold cathodes and reservoir hot cathodes. Ultimately we decided that traditional M-type dispense cathodes were the lowest risk approach. We were able to operate at high emitter density (10-20 A/cm<sup>2</sup>) that was required to achieve high power and gain. But the price for this was shorter lifetime. Ultimately an advanced cathode such as scandate will be required to provide both high current density and long lifetime.
- The cathode heater package was a significant problem throughout our multi-beam HPA program. We obtained five planar cathodes from Semicon for our tests, and all five suffered heater failures that required tube rebuilds. These planar cathodes did need heater powers significantly higher than our single beam cathodes (20 W vs 5 W), and even though our design calculations indicated that the heater package was sufficiently robust, our testing indicated otherwise. Future multi-beam amplifiers will need better cathode fabrication processes.
- Our Phase 1 beamstick with twenty-five beamlets was an extremely challenging fabrication task, and we decided to use a design based on emitting pellets that were laser-welded into a non-emitting focus electrode made of TZM. It was felt that this would provide the best chance for generating 25 well-aligned beamlets. This approach did not work well, probably because of poor thermal isolation of the emitter pellets, and barium deposition on the focus electrode. In Phase 2 the HPA was based on a five-beam design, and we designed cathodes with emitters that were physically separated from the focus electrode. This provided the necessary thermal isolation so that the emitters could reach the necessary temperature to generate the required total current of 250 mA.
- As we designed the planar gun, the size grew because of beam optics and high voltage requirements. The focus electrode cross section needed to be large enough so that edge electrostatic fields would not deflect the outermost beamlets of the array. And the outer gun can walls needed to be sufficiently far from the cathode to avoid voltage breakdown. This was particularly difficult because of the need to operate at 20 kV. Ultimately this led to a relatively large gun, which also impacted the size of the magnet bore.
- The cathode required a long molybdenum post to provide good thermal isolation. This post needed to be welded and held stably in a high voltage ceramic header. Aligning the cathode and achieving a stable weld was very challenging and required special fixtures. Although we were successful, a new support design would be desirable for future multi-beam amplifiers.

## HPA Fabrication

- Both the beamstick and the five-beam amplifier were based on a rectangular geometry. This was dictated by the high-aspect ratio of the beamlet array. The need for a vacuum-tight assembly resulted in difficult welds that were prone to cracking. Fixturing was used as much as possible to ensure uniform welding. Precise control of the laser focal point while welding around corners was especially difficult. The use of thin weld lips lowered the welding power required and increased the hermeticity yield.
- Whenever possible, brazed sub-assemblies were used. This generally resulted in fewer leaks and an easier assembly process.
- It was best to make the HPA vacuum envelope out of one material, such as cupronickel, to avoid the problems associated with different material properties. For example, we made the gun can from cupronickel and had a separate internal iron shielding assembly.

- Alignment of the electron beam with the beam tunnel axis was quite challenging. We had our best results when we imaged the beamlets at the anode with a copper foil, and used this measurement to position the carrier holding the circuit for the final assembly weld.

## Single-Beam HPA Development

### FWG Circuit

- Because a higher current density beam is required to achieve a given RF power, beam interception can cause more damage. Ideally transmission should exceed 95%. We typically selected a relatively large beam tunnel to reach this goal, with the option of moving the beam off-axis to achieve better coupling if needed. The beam would be moved off-axis by adjusting the position of the magnet. We also added a tungsten beam scraper at the circuit entrance to stop edge emission electrons from entering the FWG circuit. These electrons typically have large scalloping orbits that cause them to intercept the beam tunnel wall.
- The DRIE circuit typically has poor thermal conductivity because of the silicon. This can lead to high wall temperatures were the beam is intercepted. We have modified the fabrication process to increase the wall copper thickness to ten microns to reduce this temperature and avoid thermal fatigue. Another consequence of high wall temperatures is the diffusion of silicon into the copper. We added a thin TaN diffusion barrier between the copper and silicon to prevent this.
- The silicon wafers typically have bowing and warping that can reduce the bonding strength. This may have been a problem with the Phase 3 circuits. Future wafers will be ordered with tighter specifications on these parameters.

### Electron Gun

- A robust cathode used in NGES TWTs was utilized. The required heater power was much lower, so cathode failure was highly unlikely.
- A biased focus electrode was incorporated into the design. This was used to reduce the edge emission and improve transmission.

### Radial-Access Magnet

- The azimuthal symmetry of this magnet provides an extra degree of freedom that can be used to improve beam transmission. Fabrication is also easier compared to the planar magnet.
- EEC developed a technique to temporarily assemble the magnet and measure the error field. This allowed them to optimize the field profile before completing fabrication.

### HPA Fabrication

- Fabrication was much simpler because of the cylindrical symmetry. Welds were more uniform, and the need to rework parts was reduced.
- We developed a new alignment procedure between the electron beam and circuit based on two locking rings. One ring is centered on the beam image generated on a copper foil during bell jar tests, and the other ring is centered on the beam tunnel axis. This approach allowed to achieved alignment better than 25 microns.
- A diamond window assembly was successfully fabricated that was tight and well matched.

---

## 7.0 IMPLICATIONS FOR FURTHER RESEARCH

The HiFIVE program at NGES resulted in the successful demonstration of high power amplifiers at frequencies between 210 and 220 GHz. However, these HPAs were typically low duty devices. We attempted to increase the duty of the single-beam HPA, and did reach 3.2%, but testing was cut short by a cathode failure. So the demonstration of high average power in amplifiers based on micro-fabricated circuits is still necessary. The ongoing ViSAR program may provide that opportunity. High average power also requires beam transmission efficiencies of 95% or better. A cathode capable of generating high current densities would result in a beam with a smaller diameter and reduce the possibility of intercept loss. New scandate technology based on nanoparticles has recently become commercially available and may provide this capability. Finally, the original goal of Phase 3, namely the integration of the RF driver and HPA, was not accomplished. This could help to reduce the RF requirements of the HPA, and lead to a lighter, more compact source that would be more appealing to system developers. The continuing development of cost-effective micro-fabrication methodologies for integrating the various circuit components into a compact HPA would also be attractive. The ultimate goal would be to produce a robust amplifier that would be compatible with military-level production volumes.